

UX-1071

UNCLASSIFIED

SRI International

Phase 1 Report • May 1999

UXO DETECTION SYSTEM BY HARMONIC RADAR

SRI Project 3036

Prepared by:

Joel Kositsky
Radio Science and Engineering Division

Prepared for:

U.S. Government

Attention: Ron Stocks

Contract No. 99-C-4047

Approved:

Murray J. Baron, Vice President and Director
Radio Science and Engineering Division



UNCLASSIFIED

CONTENTS

LIST OF FIGURES iii

LIST OF TABLES v

1 EXECUTIVE SUMMARY 1

2 HARMONIC RADAR BACKGROUND 2

3 LABORATORY MEASUREMENTS 4

 3.1 TARGET SETS 6

 3.1.1 UXO 6

 3.1.2 Other Targets 7

 3.2 CW EXPERIMENTS 7

 3.2.1 Experimental Setup 7

 3.2.2 Control Software 13

 3.2.3 Experimental Procedure 17

 3.2.4 Results 19

 3.2.5 Summary and Conclusions 24

 3.3 IMPULSE EXPERIMENTS 29

 3.3.1 Experimental Setup 29

 3.3.2 Experimental Procedure 31

 3.3.3 Results 36

 3.3.4 Conclusions 37

4 VAN EXPERIMENTS 39

 4.1 RADAR VAN SYSTEM 39

 4.2 LOCAL TESTING 39

 4.3 GOVERNMENT SITE TESTS AND RESULTS 44

 4.4 CONCLUSIONS 51

5 CONCLUSIONS AND LESSONS LEARNED 57

APPENDICES

 A ORIGIN OF THIRD HARMONIC RESPONSES 58

 B UXO RCS MEASUREMENTS SUMMARY 61

 C STEPPED CW VS IMPULSE WAVEFORMS 62

UNCLASSIFIED

LIST OF FIGURES

1	Conventional vs third-order SAR.....	3
2	Anechoic chamber test setup	5
3	Back-to-back diode v/i characteristic	8
4	CW measurement system block diagram.....	9
5	Mk230 hydrostatic fuze in test area	11
6	Sleeve dipole test antenna (180 to 360 mhz)	12
7	Sandbox in anechoic chamber.....	14
8	LabView front panel.....	15
9	Data acquisition flowchart.....	16
10	E field components at maximum CW level.....	20
11	Spectrum analyzer sweep over third harmonic band.....	21
12	Third harmonic response of Mk230 vs incident power.....	22
13	Third harmonic response of ammunition box vs incident power.....	23
14	Third order harmonic response of ammunition box.....	25
15	Third order harmonic conversion frequency of mk230.....	26
16	Third harmonic response in air and in sand.....	27
17	Impulse measurement system block diagram	30
18	Band-reject filter characteristic.....	32
19	Impulse spectrum filtering	33
20	Wideband excitation and third-harmonic response	34
21	E field components with attenuated impulse excitation	35
22	Two-channel van radar block diagram	40
23	Image of buried mines at Nevada Test Site	41
24	Side-looking two-channel radar at YPG.....	42
25	Two-channel impulse radar images.....	43
26	Site layout at YPG.....	45
27	UXO in burial holes at YPG, ready for backfilling.....	46
28	Targets of opportunity at YPG.....	47

UNCLASSIFIED

LIST OF FIGURES (CONCLUDED)

29	Third harmonic background levels at YPG	52
30	Third harmonic background response variance	52
31	Third harmonic CW response of UXO not detected	53
32	Third harmonic CW response of 150M projectiles	53
33	Third harmonic CW response of horizontal Mk230s	54
34	Third harmonic CW response of vertical Mk230s	54
35	Third harmonic CW response of belted shells (perpendicular to E field)	55
36	Third harmonic CW response of belted shells (parallel to E field)	55
37	Third harmonic CW response of bomb fuzes	56

UNCLASSIFIED

LIST OF TABLES

1	UXO Items Tested.....	6
2	Sample Data Spreadsheet	17
3	CW Test Result Summary	28
4	Impulse Test Results Summary.....	37
5	New UXO Buried at YPG	48
6	CW Results Summary from YPG	49

UNCLASSIFIED

1 EXECUTIVE SUMMARY

This project was designed to ascertain the utility of harmonic radar techniques in helping with the detection and classification of buried unexploded ordnance (UXO).

Some radar targets will generate not only the conventional radar returns at the incident frequency, but also low level signals at harmonic frequencies (primarily third harmonics of the illuminating frequency). These harmonically active targets are almost exclusively metallic or electronic in composition. Usual ground radar clutter targets (rocks, ground surface, soil inhomogenities, and so on) produce virtually no harmonics, and will therefore produce no competing signals (i.e., clutter) for a third harmonic receiver.

Unfortunately, not all metal objects produce harmonics; an appropriate metal-metal interface with a thin insulator in between is required. A single pristine shell will probably not generate harmonics, but one that has been fractured, or has fins, vanes or other metal pieces, is a candidate for harmonic production. Complex UXO, such as rockets with fins, fuzes with pins, projectiles with vanes, as well as aggregates of UXO, such as a case of shells, will also be likely producers of harmonics.

We found in the laboratory that about one-fourth of the individual pieces of UXO were detectable with harmonic techniques, while about one-half of the aggregates were detectable. Burial of the test objects in sand attenuated the signals, but did not change the basic results.

Two types of harmonic radar (impulse and CW) were installed on a van to collect data from UXO under field conditions. One type, the impulse waveform system, showed capabilities of imaging harmonic targets, and led to the surprise discovery of a trip wire attached to a surrogate mine that we had no idea was in the test area. This system shows some promise as a moderate-distance standoff detector, but a lot of work would be required to develop it into a truly robust field tool. The other type of system that we deployed, a step-frequency CW system, was at least as effective as the impulse system and can be much more easily transitioned to a field-ready tool.

An important result of the work came from an analysis of the data from the CW system. Harmonically active UXO seem to have spectral "signatures," unique responses as a function of frequency, that remain identifiable regardless of burial orientation. The existence of such a signature would be invaluable for UXO identification. This preliminary result will be investigated further in the next phase of the work.

As a primary buried UXO sensor, a harmonic radar would miss too many types of targets. However, such a system can be made both small and simple enough to be included in a suite of sensors designed for buried UXO detection and identification. As such, a harmonic radar would add a valuable new source of information for addressing this difficult challenge.

UNCLASSIFIED

2 HARMONIC RADAR BACKGROUND

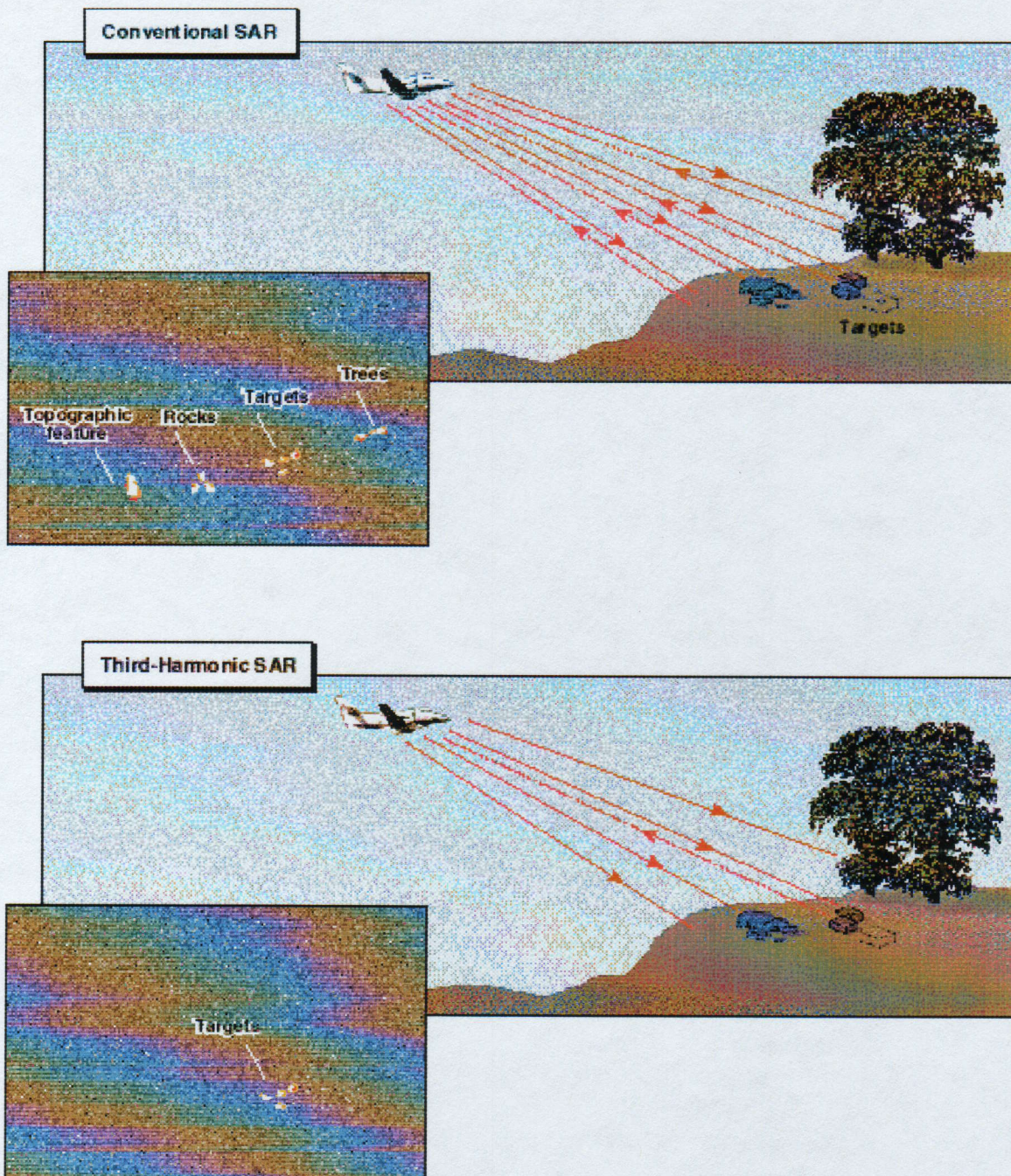
The concept of a radar that detects only man-made metallic objects by monitoring third harmonic reradiation was conceived over 25 years ago. Such a radar would be a powerful tool, capable of discriminating among metallic targets and natural clutter at the phenomenological level. Although previous implementations proved the fundamental concepts, they also revealed a major stumbling block: the available power levels typically limited the standoff range of third harmonic radars to distances that were unacceptably short for most military applications.

UXO detection in the Continental US (CONUS) does not require large standoff distances. In fact, most of the detection tools, such as magnetometers and metal detectors, are proximity sensors. Harmonic radar was, therefore, revisited for this application.

The physical basis of third harmonic radars lies in the electrical nonlinearities of metal-metal joints caused by impurities (usually oxide layers) in the junctions. When such junctions are electrically excited at a given frequency, they reradiate energy not only at the incident frequency (the basis of conventional radars), but also at harmonic frequencies. (A mathematical derivation of harmonic production is sketched out in Appendix A.) Most metal-metal junctions, such as those found on vehicles, generators, buildings, munitions, and so on, tend to reradiate not only at the fundamental frequency, but also at odd harmonics, with the third harmonic typically being the strongest (nonfundamental) frequency. Since virtually all natural objects (trees, rocks, topological features, etc.) reradiate only at the incident frequency, exploitation of the third harmonic reradiation phenomenon should result in a radar that detects only targets with the appropriate metal junctions.

Figure 1 conceptually illustrates the difference between a conventional and a third harmonic synthetic aperture radar (SAR) on an airborne platform. In Figure 1a, the targets as well as the clutter objects in the scene reradiate energy at the same frequency as the incoming energy. This conventional radar detects all the scatterers in the scene producing an image in which it is difficult to discriminate the targets of interest from the clutter. In Figure 1b, only the metallic targets reradiate energy at the third harmonic frequency, so that a radar receiver tuned to this (higher) frequency band will detect and image only the targets.

While an airborne implementation would have the advantage of wide-area survey capabilities, it has the difficulty of generating sufficient power density at the target inherent in standoff harmonic radar. Harmonic sensors operating in close proximity to the potential target is both appropriate in the UXO detection arena, and technically feasible. Many UXO items possess metallic joints (at fins, pins, rings, vanes, etc.) that are potential sources of nonlinearities that produce harmonics. Many pieces get fractured or mushroomed upon entering the soil, while others may rust in the ground producing potential sites of harmonic generation. Aggregates of buried metal items would also have the necessary metal-metal interfaces to be active harmonically. This project was designed to ascertain the utility of harmonic radar in the detection and classification of buried UXO.



486-115/11

Figure 1 Conventional vs third-order SAR.

3 LABORATORY MEASUREMENTS

Data were initially collected in a laboratory environment to measure typical levels of third harmonic energy produced by illuminating UXO samples. Controlled experiments were also performed to ascertain what frequencies, waveforms, polarizations, and energy levels would optimize detection.

The general experimental setup is illustrated in Figure 2. A signal at a fundamental frequency f_1 , filtered to contain no detectable third harmonic energy, was radiated at the target UXO (device under test [DUT]) by a transmit antenna. A receive antenna collected a portion of the third harmonic energy, at f_3 , three times the fundamental frequency generated by the DUT, and sent it to a calibrated receiver where it was measured and logged on a computer. The DUT, transmit and receive antennas were placed in one of the contractor's electromagnetically shielded "anechoic" chambers to isolate the third harmonic reradiation from competing ambient signals. The chamber was enclosed in a sealed metal box with a metallic door for access. The chamber is lined with radar-absorbing material (RAM) on all six sides (walls, floor, and ceiling) to isolate any chamber wall effects from the test space. The RAM was effective down to about 180 MHz for these experiments.

Several issues were important in designing the experiments. Since third harmonic energy levels were anticipated to be very low, a very sensitive system had to be assembled. Dynamic range was of paramount importance in measuring these low signals in the presence of the large transmit signals as well as the ambient. The anechoic chamber had to be tested and modified to diminish harmonic generation by loose metal-to-metal contacts. The transmit signal itself had to be very pure (i.e., contain very low levels of third harmonics), which required designing special antennas, filters, and connectors that would not generate any spurious harmonics.

To overcome the very low third harmonic conversion efficiencies that were anticipated, we pursued two strategies to increase the all-important signal-to-noise ratio (SNR). One approach was to increase the SNR by decreasing the thermal noise level. This was done by radiating a CW narrowband fundamental frequency and then employing a very narrowband receiver. A second approach aimed at increasing the third harmonic signal by using a very high peak power (impulse) excitation source, at the price of a wideband (high thermal noise) receiver. The details of the experimental procedure and equipment were different for the two waveforms used, and will be discussed individually in Sections 3.2 and 3.3, following a discussion in Section 3.1 of target sets used in these experiments

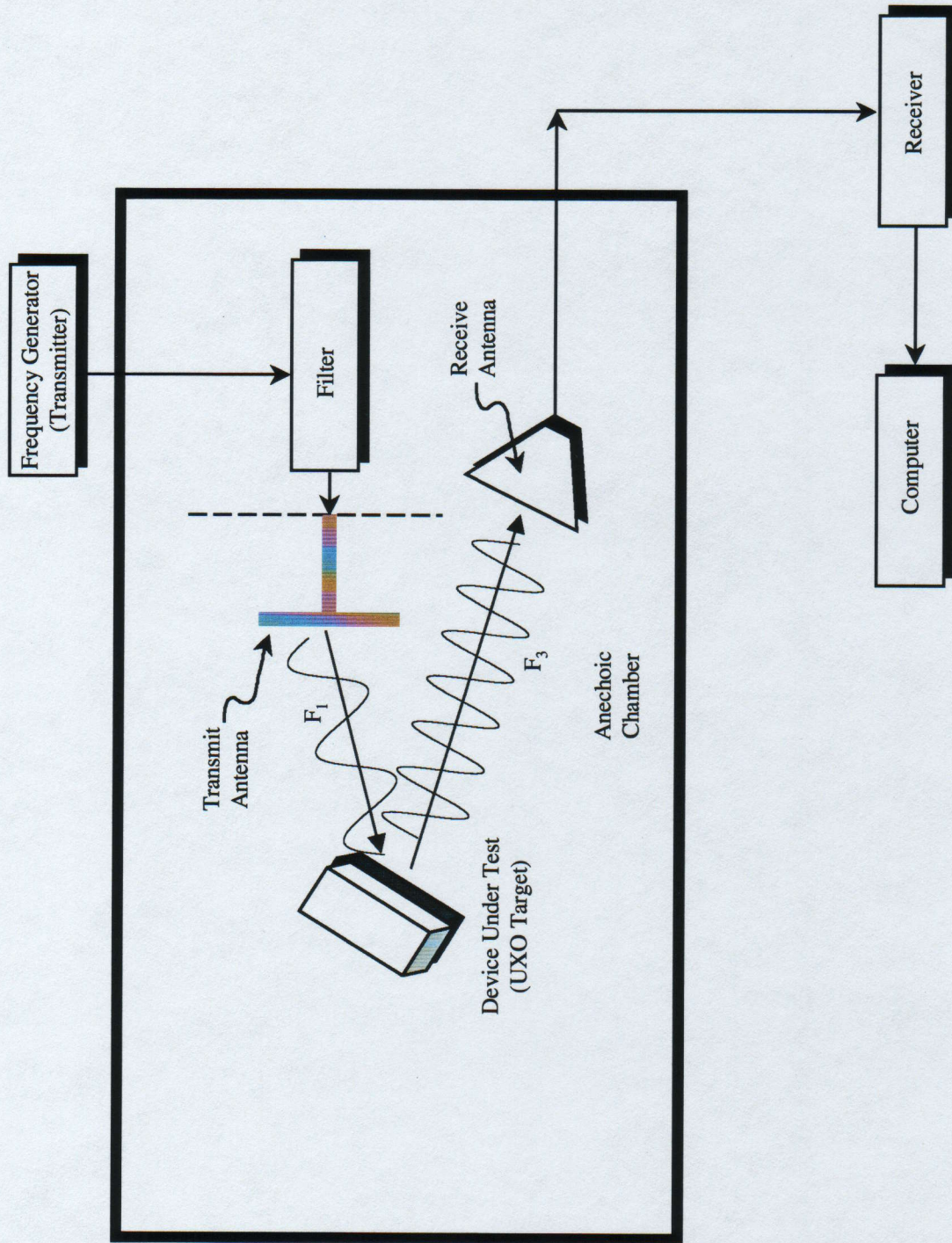


Figure 2 Anechoic chamber test setup.

UNCLASSIFIED

3.1 TARGET SETS

3.1.1 UXO

A set of UXO was chosen from the collection at the Yuma Proving Ground (YPG) and shipped to SRI. This set of targets, while necessarily incomplete, was chosen to reflect a cross section of typical UXO, varying in size (individual rifle shells to a 250 lb bomb casing), complexity (empty shells to hydrostatic fuzes), and state of wear (pristine to rusted and mushroomed). Where practical, a minimum of three examples of each type of UXO were used to test for consistency of response. A total of over 100 pieces, representing over 20 types of UXO were chosen. These items are shown in Table 1 below. All items were labeled with a name consisting of an abbreviation of the UXO type and a letter to distinguish duplicates of any particular type of UXO.

Table 1
UXO Items Tested

Designator	Description	Quantity
Mk230	Hydrostatic Fuze	3
FZ2.75	2.75" Fuze	3
XM229	2.75" Warhead	3
Mk40	2.75" Rocket	3
M80	Grenade	5
M42	Grenade	5
G811	Grenade Body	10
M879	81 mm Practice Mortar	3
M97	Blu	3
Rock	Rock Eye	3
91B	Volcano 91B	3
Vol	Volcano Cannister	3
Mk45	Flare	3
60mm	60 mm Mortar with Fins	3
105	105 mm	3
B250	250# Bomb Case	1
Mk106	Practice Bomb	3
Mk76	25# Practice Bomb	3
M103	20 mm M103 Practice with Cartridge	4
40	40 mm Projectile	3
	Assorted Small Arms (brass)	Many
	Ammo Box	1

UNCLASSIFIED

3.1.2 Other Targets

Other targets were also used during experimentation. Several types of landmines (although not a constituent of the CONUS UXO target set) that were at SRI were used as targets while we awaited the UXO shipment from YPG. Other "generic" third harmonic producers, such as a wad of steel wool and a cardboard box of joist hangers, were used to test the experimental setup.

Since the harmonic response of many objects varies with time, because of changes at the nonlinear metallic joints, we built a special third harmonic target whose response was stable. This target consisted of a pair of back-to-back diodes attached to a dipole antenna. The stable voltage/current (V/I) characteristic of back-to-back diodes is shown in Figure 3 below. A pure cubic V/I characteristic (that of an optimal third harmonic generator) is shown as a dotted line in the figure. As can be seen, the back-to-back diodes have a large third-order term making them efficient harmonic generators.

This type of calibration target is very stable since it relies on a solid state V/I characteristic rather than the fortuitous metal-oxide-metal spacing of other harmonically active targets. As such, this target was used extensively to gauge the stability of the experimental setup. At times attenuators were used between the antenna and the diodes to decrease the large response of the target to levels more typical of UXO.

3.2 CW EXPERIMENTS

Of the two transmit waveforms that we used in this work, the CW waveform was the easiest one to both implement and interpret. We therefore started with this approach for our laboratory tests.

3.2.1 Experimental Setup

Figure 4 shows a block diagram of the CW experimental setup. An HP8656B frequency generator created the fundamental frequency waveform. This signal was passed through a low-pass filter to remove any third harmonic spurious signals produced by the frequency generator, before the signal was passed to a 60 dB (100 watt maximum) linear amplifier. This power amplifier was gated to produce a pulsed CW signal in order to decrease the average power being generated. The amplified signal was low-pass filtered and fed to a linearly polarized wideband dipole antenna located in the anechoic chamber.

On the receive side, a commercial dual-ridged (linearly bipolarized) antenna was used to receive the reradiated energy. Since this antenna is exposed to reflections that are many orders of magnitude stronger at the fundamental frequency than at the third harmonic, it was imperative

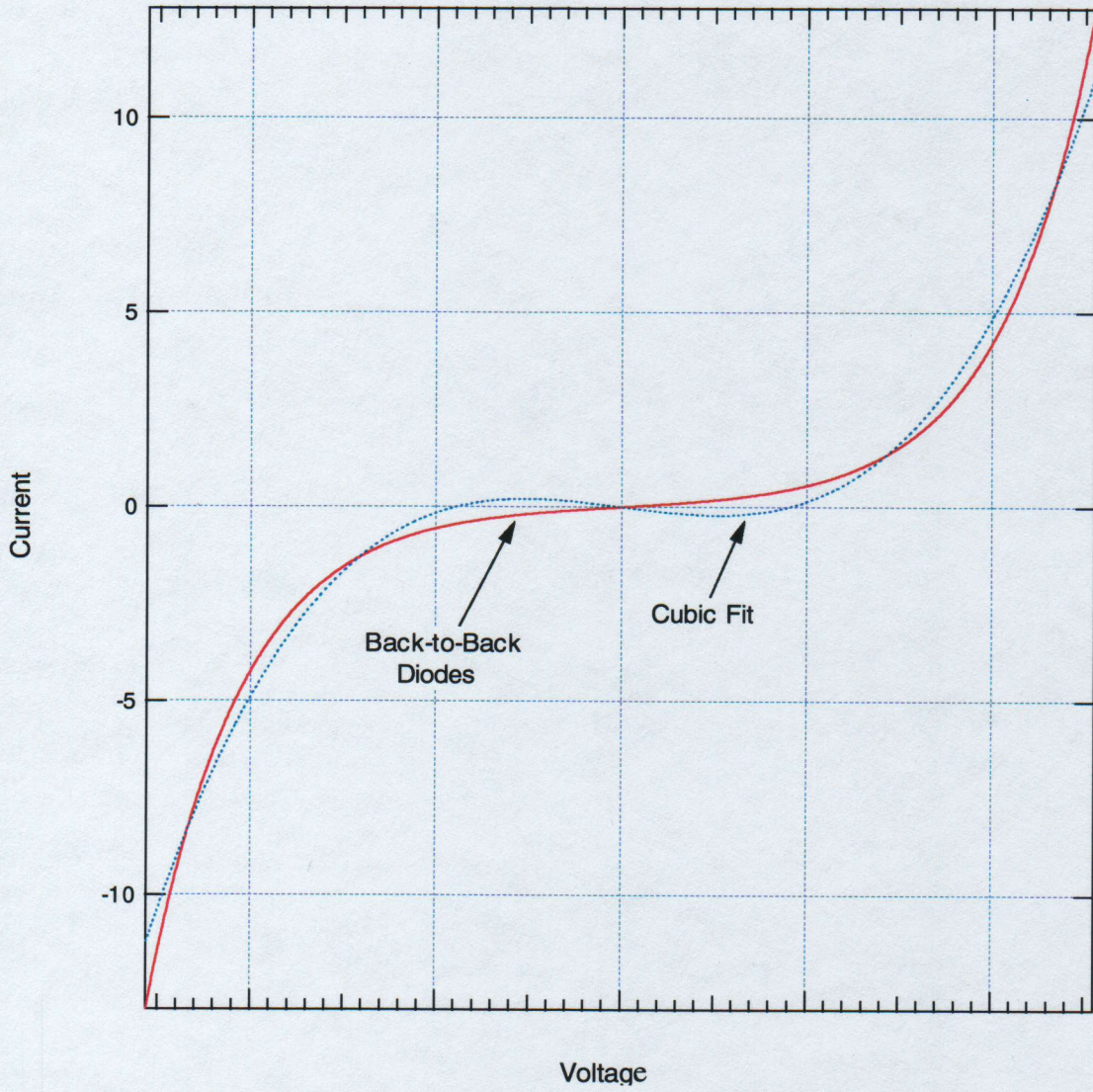


Figure 3 Back-to-back diode V/I characteristic.

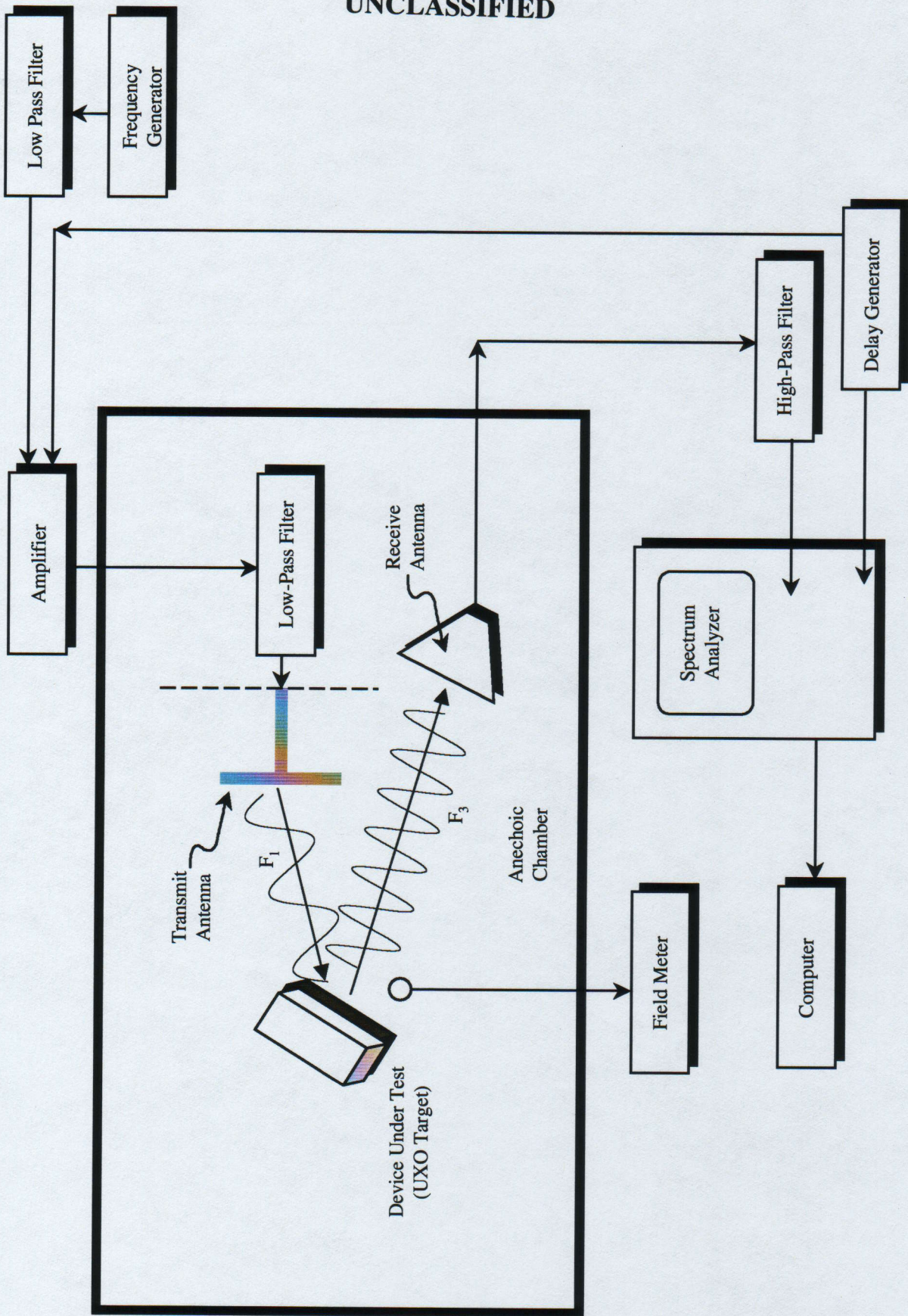


Figure 4 CW Measurement system block diagram.

UNCLASSIFIED

to filter the primary frequency as early in the receive chain as possible, so that third harmonics would not be produced in the receive antenna or connectors. A small horn with cut-off well above the fundamental frequency was therefore selected, to decrease the coupling to the primary frequency energy. For the same reason, the receive signal was high-pass filtered before being fed to the spectrum analyzer that acted as the receiver.

We used an HP8566B spectrum analyzer (SA) to detect the signals. In order to decrease the thermal noise of the receiver, we preceded the SA with an HP85685A tracking preselector. With this setup we could measure signals to as low as -120 dBm with excellent SNR, in a 20 ms sweep time. The maximum power level and its frequency were then (automatically) noted and written to a data file.

Synchronization of the power amplifier gating and the SA sweep triggering was accomplished using an SRS DG35S digital delay generator. An electric field probe and meter were optionally used in system calibration and testing.

Figure 5 shows an Mk 230 in the anechoic chamber ready for testing. Note the blue pyramidal RAM in the background.

Custom Components. Wherever possible, we used existing laboratory equipment. Third harmonic work, however, presents unique challenges that need to be met with custom solutions. This was especially true in the transmit chain, where high-power signals typically produce nonnegligible levels of third harmonics in threaded and other connectors, as well as at mechanical metal joints in the transmit antenna. These spurious harmonic signals can be high enough to mask any harmonic signals produced by the DUT.

We therefore took great care in designing, fabricating, and assembling the transmit filters and antennas. In the CW case, we were able to procure a number of commercially available low-pass filters that could handle the transmit power and could be soldered directly to the antenna feed. The antenna design was based on a wideband sleeve-dipole concept.¹ It was carefully assembled so that all metallic joints were soldered. Figure 6 shows a schematic of the dipole design. The dipole arms were made from two brass pipe sections. The solid jacket coaxial feed cable was soldered to one of these dipole arms while the solid center conductor was soldered to the other arm. The balun consists of several ferrite beads that were slipped over the coax as close to the feed points as possible. This simple balun works by suppressing RF currents on the outer surface of the coax. The sleeves were made from brass pipes of the appropriate diameter, fixed with nylon screws to dielectric spacer rings that slipped over the radiating arms. The antenna was tested for RF properties and was found to perform well over an octave bandwidth (180 to 360 MHz).

¹ See Johnson and Jasik, *Antenna Engineering Handbook*, McGraw-Hill, New York, 1961.

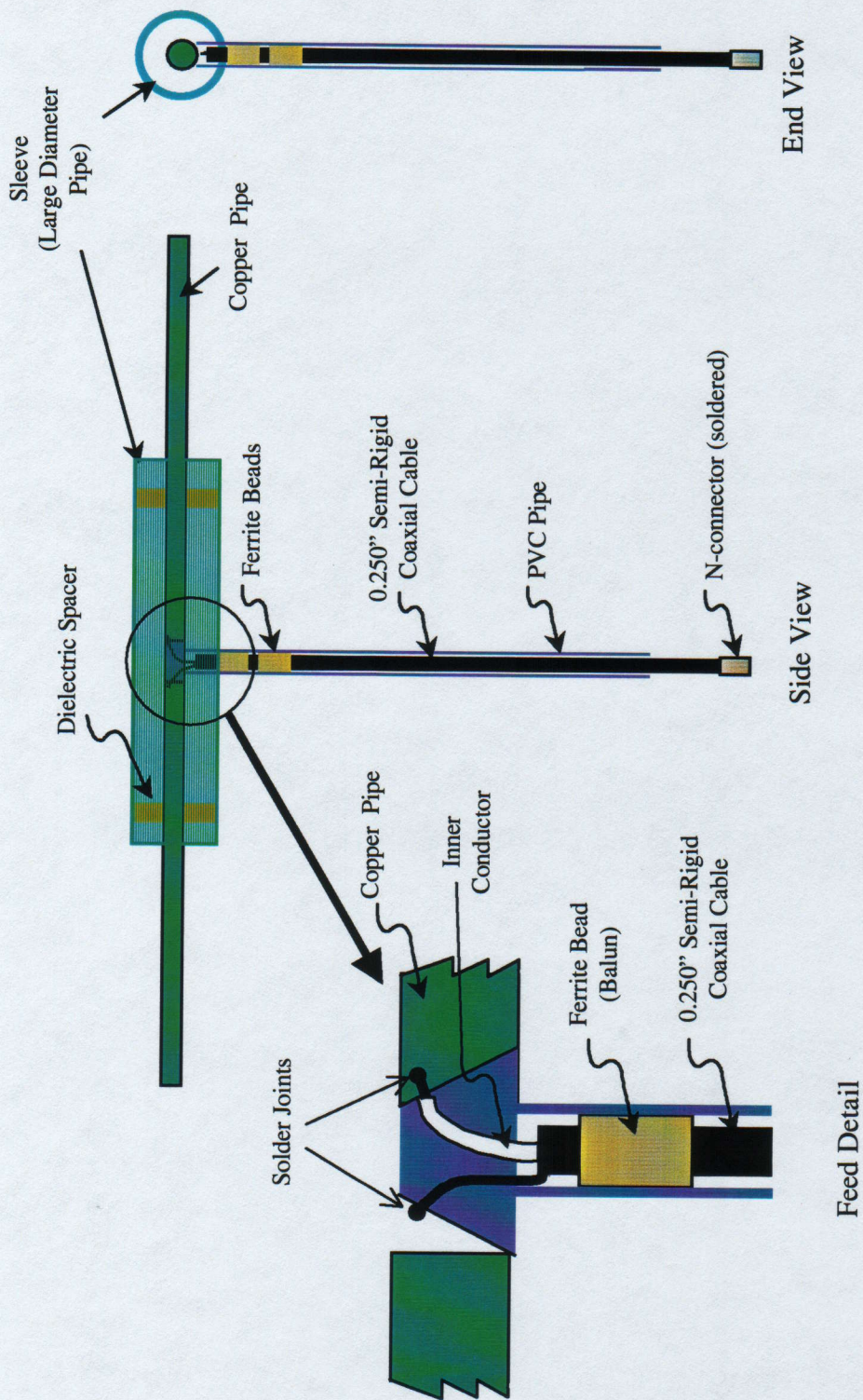
UNCLASSIFIED



Figure 5 Mk230 hydrostatic fuze in test area.

UNCLASSIFIED

UNCLASSIFIED



End View

Side View

Feed Detail

Figure 6 Sleeve dipole test antenna (180 to 360 MHz).

UNCLASSIFIED

Sandbox. In order to verify that harmonic effects would be similar for buried and in-air targets, a sand-filled test box was built inside the anechoic chamber. Figure 7 shows a photograph of the box inside the anechoic chamber. The box was made of plywood and lumber, glued and/or doweled together without the use of any metal that might interfere with the test measurements. A partition divided the 40"× 40"× 8' box into two roughly cubic volumes, one of which was filled with dry river sand.

During sandbox testing, the same piece of UXO would be placed on a styrofoam pedestal in the empty half, or be buried in the sand in the other half. In this way, we were able to obtain comparative measurements for in-air or in-sand third harmonic responses.

3.2.2 Control Software

The data collection was placed under computer control using LabView and the GPIB interface. A custom LabView program was written to accomplish the data acquisition and logging functions in an automated fashion.

Figure 8 shows the front "panel" of the LabView program. The user typically enters the start, stop, and frequency increment of the desired fundamental frequency range; the start, stop, and power increment of the desired transmit levels; the number of repetitions of each of the measurements desired; the desired receive polarization(s); as well as a file name. The program prompts for a DUT name from the list of available UXO and constructs a file name incorporating the date, the user-supplied name, and the UXO under test. The operator can also specify the number of sweeps desired if data pre-averaging is being used, and the number of times (loops) the whole sequence should be repeated.

The data acquisition sequence is shown in Figure 9: The frequency and amplitude are set on the frequency generator. The power level is stepped from the initial to the final levels at each frequency. The frequency is then stepped through its range according to the operator-selected values. At each combination of frequency and power level, the power amplifier is gated while the SA analyzes the level of the third harmonic response for a given polarization. The results are written to an Excel spreadsheet for later analysis.

Table 2 shows an example from a spreadsheet containing data from a typical data run. The file name (Cal Dipole Oct_15.xls) shows that the data were collected on 15 October with the DUT being the calibration target attached to a dipole. The columns list the transmit polarization (H in this case); Greenwich Mean time; loop number (for multiloop data); fundamental frequency (MHz), and power level (dBm) set on the frequency generator; the number of sweeps that were used for averaging, the third harmonic response level (dBm), and the frequency of the peak response (MHz) for H, and then V receive polarizations; and the amount of leakage (and the peak frequency) of the fundamental energy. The last columns were optionally used during calibration runs when an electric field sensor was used to characterize the power levels at the DUT site.

UNCLASSIFIED

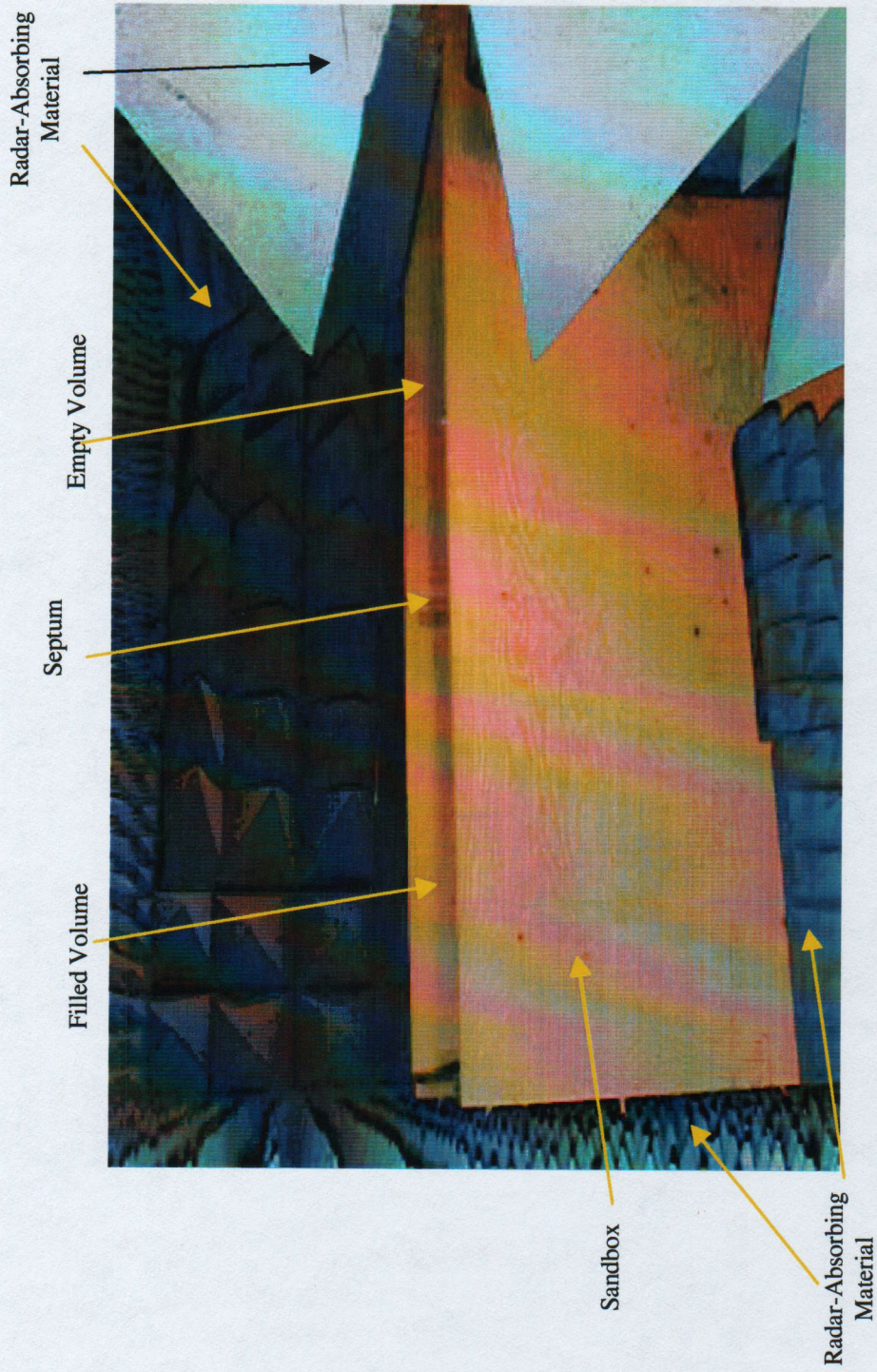


Figure 7 Sandbox in anechoic chamber.

UNCLASSIFIED

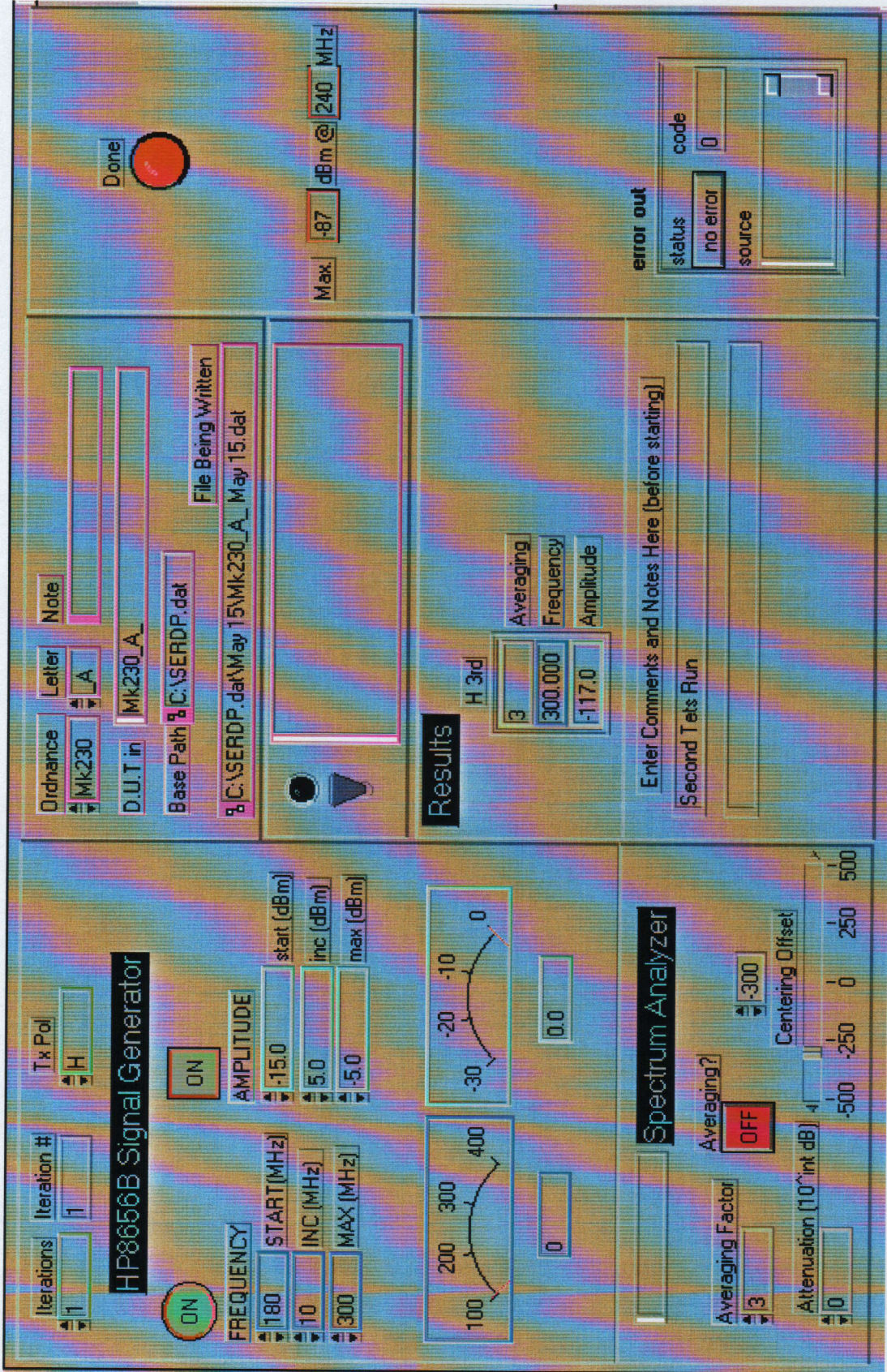


Figure 8 LabView front panel.

UNCLASSIFIED

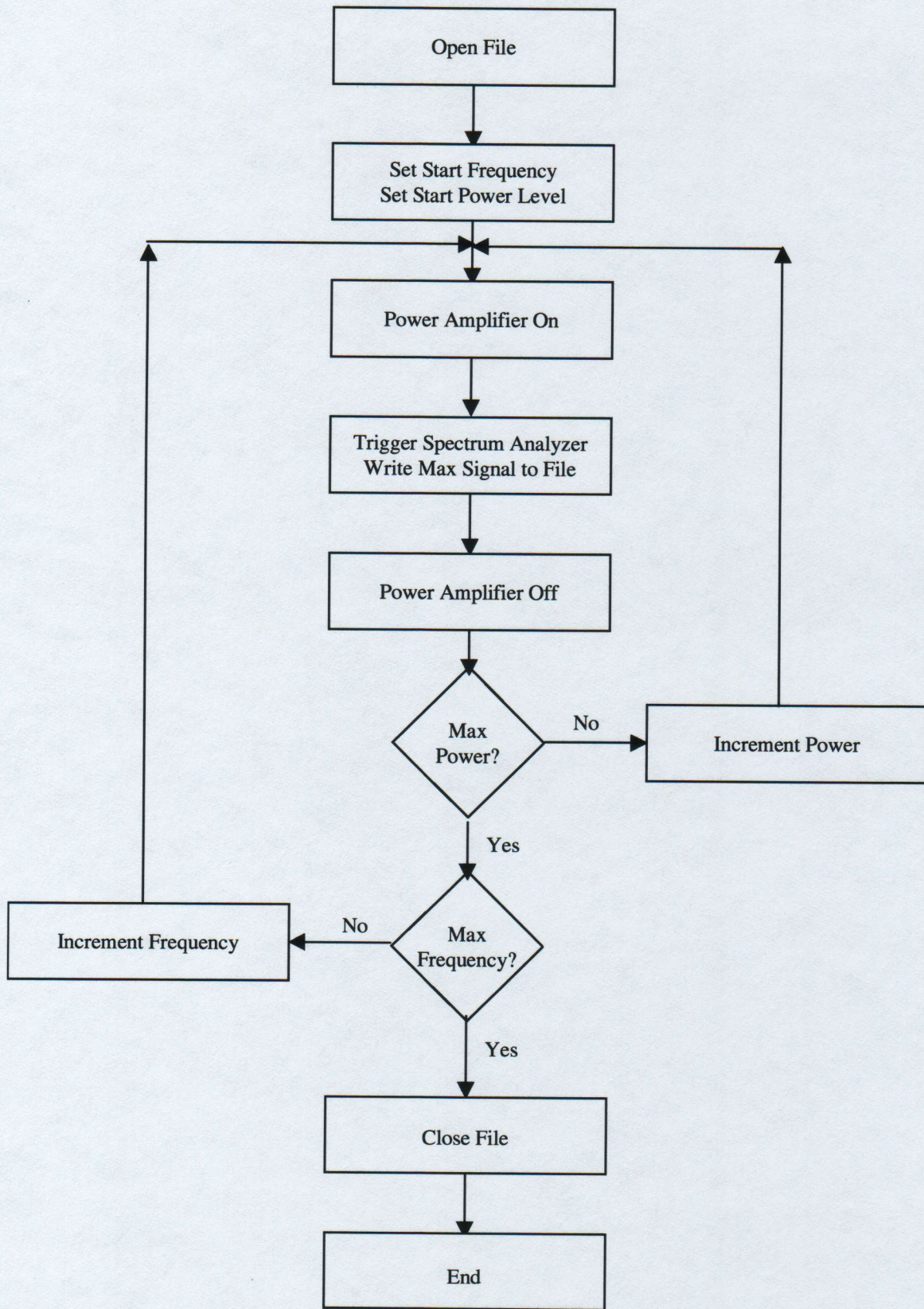


Figure 9 Data acquisition flowchart.

UNCLASSIFIED

UNCLASSIFIED

Table 2

Sample Data Spreadsheet

0 = H-pol	Time	Loops	Frequency (MHz)	Power Level (dBm)	Averaging	THR H-pol	Peak Freq (H)	Average	THR V-pol	Peak Freq (V)	Fundamental	Peak Freq		
0	2959792955	1	190	-5	1	-91	570.0	1	-96	570.0	-48	190.0	0	0
0	2959792969	1	200	-5	1	-95	600.0	1	-105	600.0	-48	200.0	0	0
0	2959792982	1	210	-5	1	-94	630.0	1	-99	630.0	-48	210.0	0	0
0	2959792995	1	220	-5	1	-84	660.0	1	-91	660.0	-51	220.0	0	0
0	2959793009	1	230	-5	1	-85	690.0	1	-96	690.0	-51	230.0	0	0
0	2959793022	1	240	-5	1	-90	720.0	1	-99	720.0	-57	240.0	0	0
0	2959793035	1	250	-5	1	-97	750.0	1	-105	750.0	-60	250.0	0	0
0	2959793048	1	260	-5	1	-94	780.0	1	-104	780.0	-64	260.0	0	0
0	2959793062	1	270	-5	1	-85	810.0	1	-96	810.0	-72	270.0	0	0
0	2959793075	1	280	-5	1	-88	840.0	1	-108	840.0	-59	280.0	0	0
0	2959793088	1	290	-5	1	-89	870.0	1	-109	870.0	-63	290.0	0	0
0	2959793102	1	300	-5	1	-98	900.0	1	-99	900.0	-55	300.0	0	0

CAL DIPOLE Oct_15.xls

The operator was informed of harmonic response levels in real time. The spreadsheet data were analyzed in more detail in post-processing.

3.2.3 Experimental Procedure

The target location and the transmit and receive antenna sites were chosen in the anechoic chamber so that

- The target volume² was uniformly illuminated by the transmit antenna
- The target volume had uniform coverage by the receive antenna
- There was over 100 dB of isolation between the transmit antenna at F₁ and the receive antenna at F₃
- The chamber walls did not produce detectable levels of third harmonics.³

Additional isolation was provided by judicious placement of RAM and single sheets of aluminum in the chamber.

² Standing waves are typically present in an anechoic chamber, so it was important to define and keep a test geometry.

³ At frequencies below about 180 MHz, the isolation was not sufficient, so experiments were primarily conducted above this level.

UNCLASSIFIED

Once the geometry of the components in the chamber were satisfactorily fixed, the system was calibrated and data were collected on the various UXO items.

CW System Calibration. One of the objectives of the CW experiments was to quantify the conversion efficiency (see Appendix B) between the incident E field on a piece of UXO and the resulting reradiated third harmonic E field. In order to calculate this conversion efficiency, we needed to calibrate the test chamber. In particular, three pieces of information were required:

- The transfer function between the fundamental frequency RF source and the resulting E field at the target location
- The E field distribution and polarization over that region
- The transfer function between the third harmonic frequency E field generated at the target location, and the measured power at the SA.

First, background measurements were made to verify that the test jig and anechoic chamber were not producing measurable levels of energy in the third harmonic band. Two types of background tests were performed: (1) tests with a 24" metal sphere at the target test site, and (2) tests with the chamber empty of all targets. A metal sphere is a well-understood, calibrated reflector of RF, but will not produce any harmonics. The sphere tests were used to verify that the level of third harmonic energy being produced and radiated by the transmit chain was below the noise, while the empty chamber measurement verified that no third harmonic processes from the chamber walls or other components were reradiating harmonics.

Once a low background signal was achieved, we measured the E-field components at the target location by using a calibrated E-field meter. This battery-powered meter was connected to the externally positioned receiver via an optical fiber link to minimize field perturbations by the probe system. In operation, all three components of the E field were measured as a function of frequency and power level at the frequency generator. The measurement data were processed to find the desired transfer function.

To test field uniformity, the probe was repositioned in the UXO target volume and measurements were repeated. The target test volume was measured to have less than a 3 dB power variation, in each of the E field components, and in the total E field. At the same time, we confirmed the linearity of the resulting E field at the target area as a function of amplitude level set at the frequency generator.

The transfer function between the third harmonic frequency E field generated at the target location and the power measured by the SA required using a test antenna of known directivity at the third harmonic frequencies. This antenna was placed at the target volume and pointed at the receive antenna. We then noted the RF power on the SA as a function of known power into the test antenna. From these data, we calculated the response of the system for a given E field in the third harmonic band, originating at the target area.

UNCLASSIFIED

These calibration steps allowed us to calculate the third harmonic conversion efficiencies of DUTs placed at the target site in the chamber from the third harmonic radar data. It should be noted that the conversion efficiencies thus calculated assumed that the objects (UXO) were isotropic radiators at the third harmonic frequency. Whereas this assumption is usually incorrect (UXO are typically cylindrical and will have angular dependencies), the absolute efficiencies will probably be good to within 5 dB, and the relative efficiencies as a function of frequency and power levels should be correct.

Figure 10 shows the measured E field components at the target location with the transmit antenna E_y polarized. Most of the E field at the target is in the E_y component, although a major E_x component is present because the target is not on boresight. The E_z component is quite small, as it should be.

UXO CW Test Procedures. Once the system was stable and calibrated, each individual piece of UXO was placed at the target site in turn, and measured for its third harmonic response. Typically, the frequencies were scanned from 190 to 300 MHz, in 10 MHz steps, with the frequency generator set at -5 dBm (resulting in the maximum peak amplified power of about 50 to 100 watts). If no third harmonic response was noted, the UXO was removed and another item was tested. If a third harmonic signal was seen, a more extensive test would be run, varying power over about 15 dB, in 3 dB increments (as well as varying frequency). Most of the UXO items were tested in several orientations as well as in aggregates.

Figure 11 shows a spectrum analyzer trace of the target response over a very large frequency range. Note the fundamental frequency leak-through at 270 MHz, and the third harmonic response at 810 MHz. A smaller second harmonic is also present at 540 MHz. In typical experiments, only the third harmonic was collected at a very narrow bandwidth.

3.2.4 Results

As shown in Appendix A, the slope of an ideal third harmonic producer should show a cubic relationship between power out at the third harmonic and power incident at the fundamental frequency. On a log-log plot, this would result in traces of slope, 3. Figure 12 shows a graph of the third harmonic response, at several fundamental frequencies, of a hydrostatic fuze (Mk 230) as the target. Note the slopes are very close to 3 as expected. Figure 13 shows a similar graph of the third harmonic response of the ammunition box to varying transmit power levels at frequencies from 240 to 300 MHz. Almost all the traces start at the noise floor (-125 dBm) and rise with a slope very close to 3, showing the expected cubic dependency. Note that the magnitude of the third harmonic signal drops as much as 25 dB over this frequency span.

UNCLASSIFIED

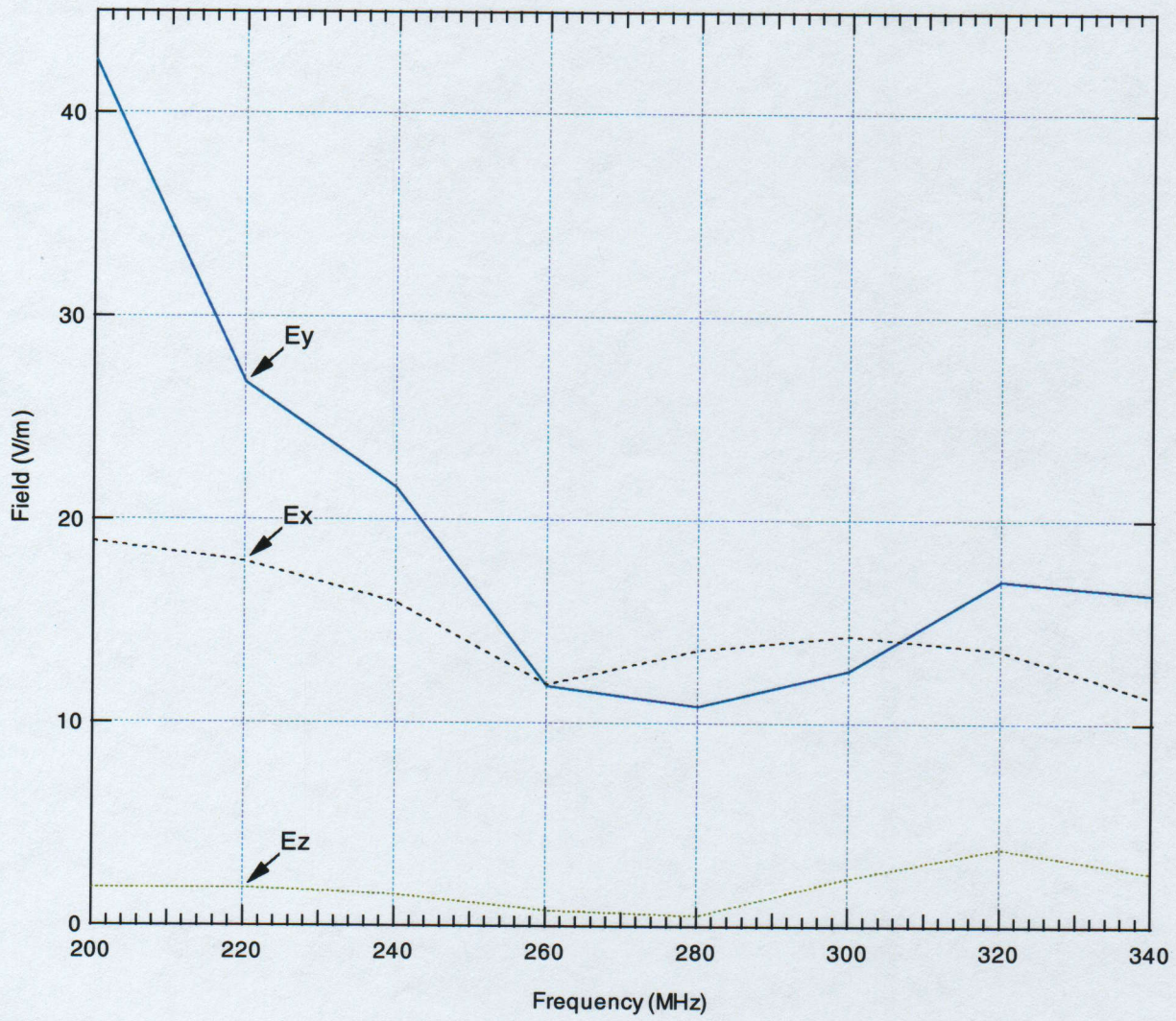


Figure 10 E field components at maximum CW level.

UNCLASSIFIED

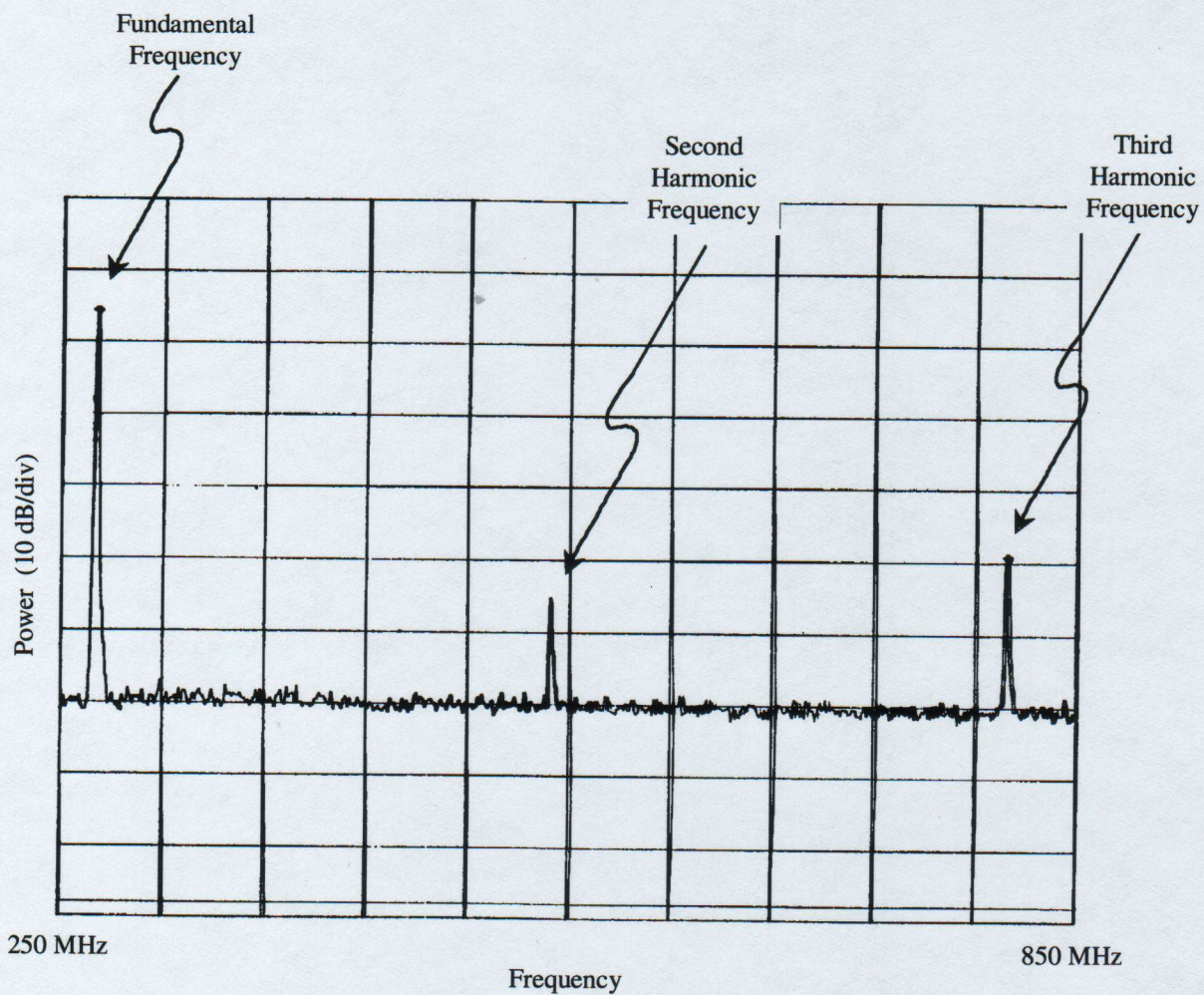


Figure 11 Spectrum analyzer sweep over third harmonic band.

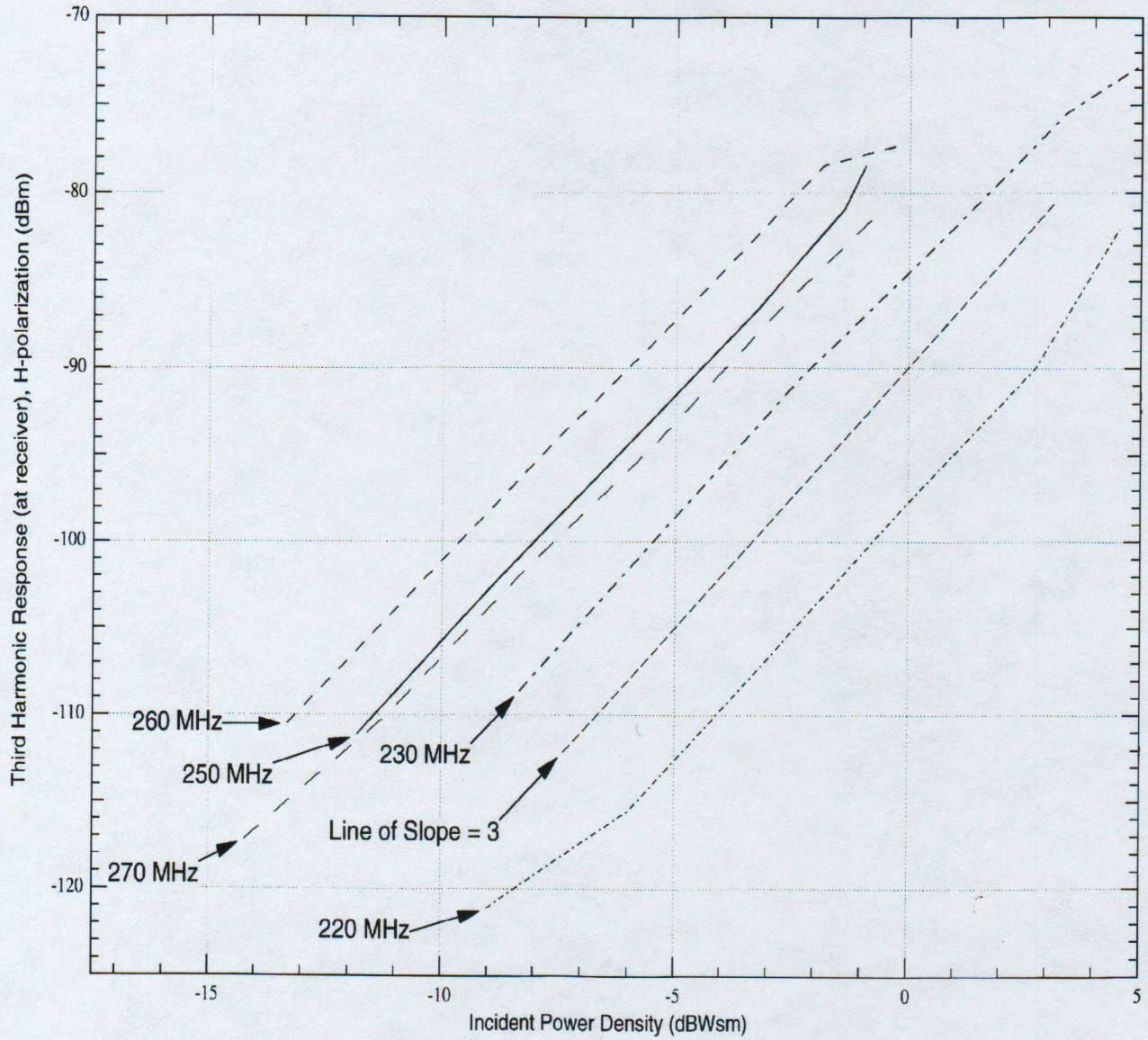


Figure 12 Third harmonic response of Mk230 vs incident power.

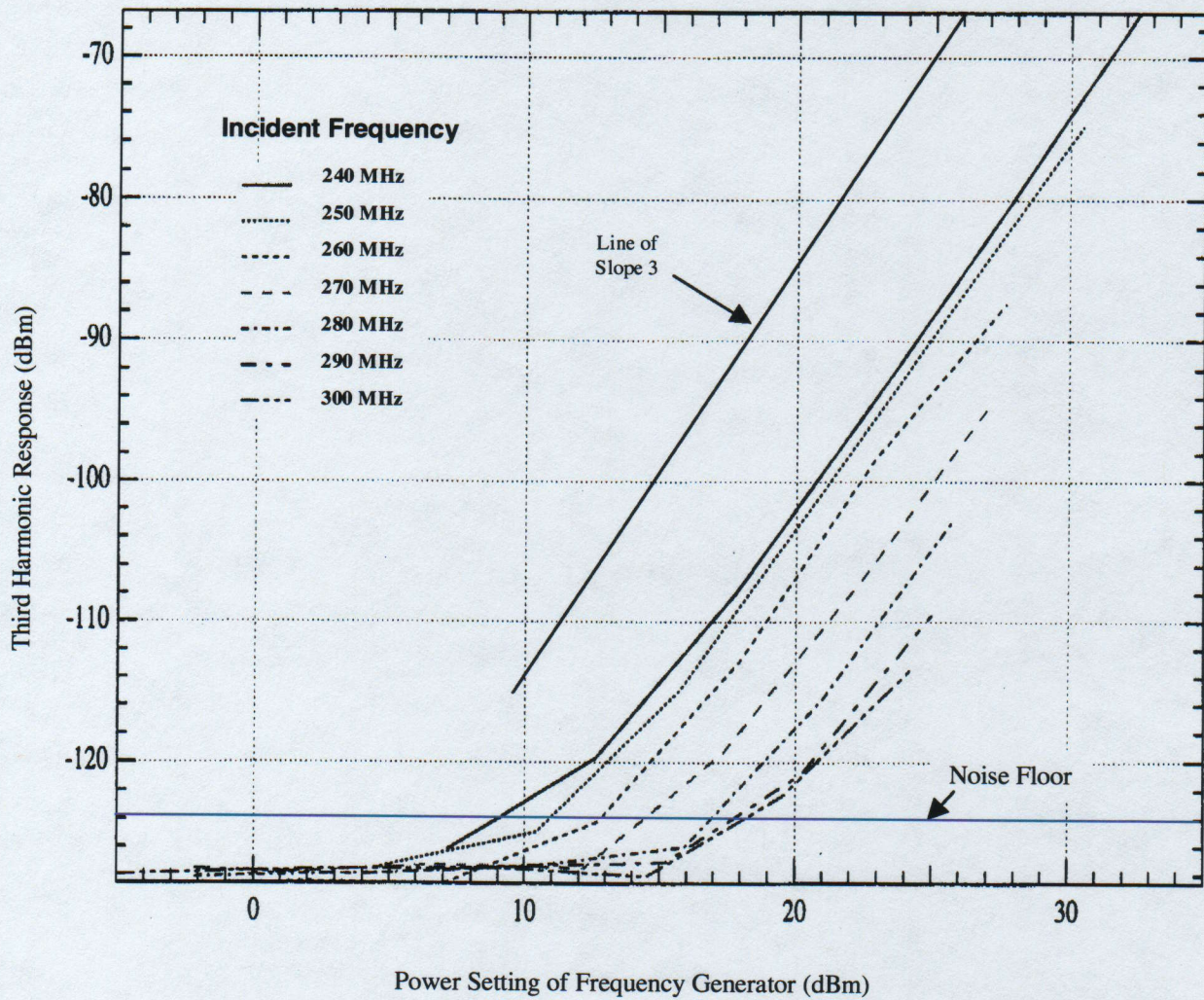


Figure 13 Third harmonic response of ammunition box vs incident power.

UNCLASSIFIED

The variation of response with frequency is plotted in Figure 14 for the ammunition box. The individual traces are lines of equal input power. The variation as seen here (up to 25 dB) with frequency, is suggestive of a target signature, an effect that might be exploited for identification. Time variations of third harmonic signals are, however, typically within ± 5 dB or even more so that "signatures" may vary temporally. A different "signature" is evident in the plot of the Mk 230 conversion efficiency vs frequency as shown in Figure 15. Here the variations with frequency are also large (about 30 dB over a 120 MHz range).

The frequency dependence seen in harmonic responses of objects is a result of two effects: First, the coupling of energy into and out from the target is frequency dependent, with higher frequencies typically coupling better (although resonance effects are almost always present). Second, the capacitive shunting of harmonic RF near the active joints tends to diminish the radiated harmonic energy. For many targets, the 100 to 400 MHz frequency range seems to optimize harmonic production.

Since the coupling has a major effect on the harmonic response, buried UXO will probably have a frequency "signature" that varies with soil condition. This effect could probably be modeled and used to predict the signature of a given UXO for a given soil matrix.

At some point, the cubic relationship, as seen in Figures 12 and 13, must level off (we can never get more energy out than we put in). This effect was seen in our experiments with the stronger harmonic targets. Figure 16a shows the response of the calibration target and Figure 16b shows the Mk 230 fuze, each in sand and in air when excited by a CW fundamental frequency. The curves begin with a slope of about three (note the different scales) and then level off at higher power levels. In these examples, the in-sand curves parallel the in-air curves very well, being offset by about 5 to 10 dB. Other examples confirmed that buried UXO (at least in dry sand) behaved very similarly to in-air UXO.

3.2.5 Summary and Conclusions

CW Results Summary. Table 3 lists a summary of the CW test results. In the table, the maximum third harmonic response, as measured on the SA, of each type of UXO is noted. When no response was measured, the response of the item is shown as "<NF"—that is, less than the noise floor.

An "X" in a column indicates whether the detection was made with individual items, or only with aggregates of the item. Obviously, items that were harmonically detected individually were also detected in aggregates.

As seen in the table, of the 23 UXO types supplied for testing, 11 produced measurable third harmonic responses in the test frequency range. The largest response (-64 dBm) resulted from stacking the 60 mm mortars. Individually these mortars were not detectable. Two of the three

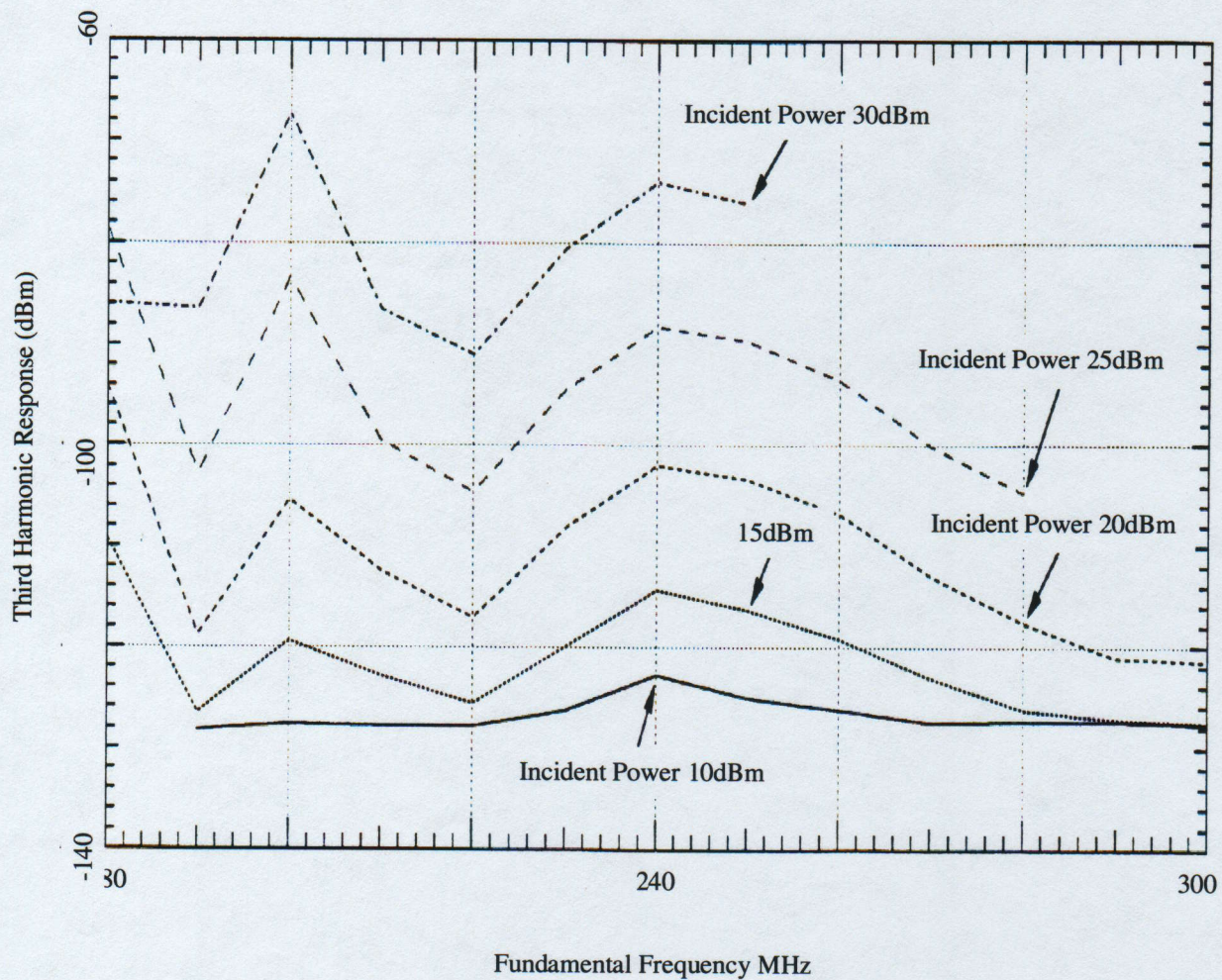


Figure 14 Third-order harmonic response of ammunition box.

UNCLASSIFIED

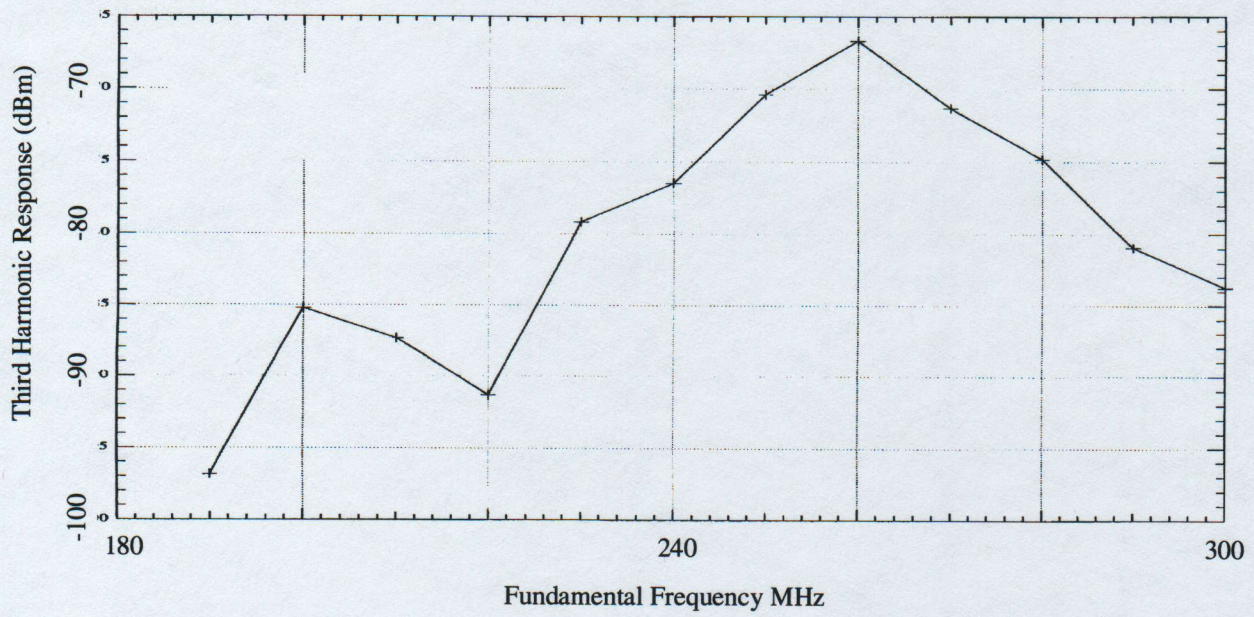


Figure 15 Third-order harmonic conversion efficiency of Mk230.

UNCLASSIFIED

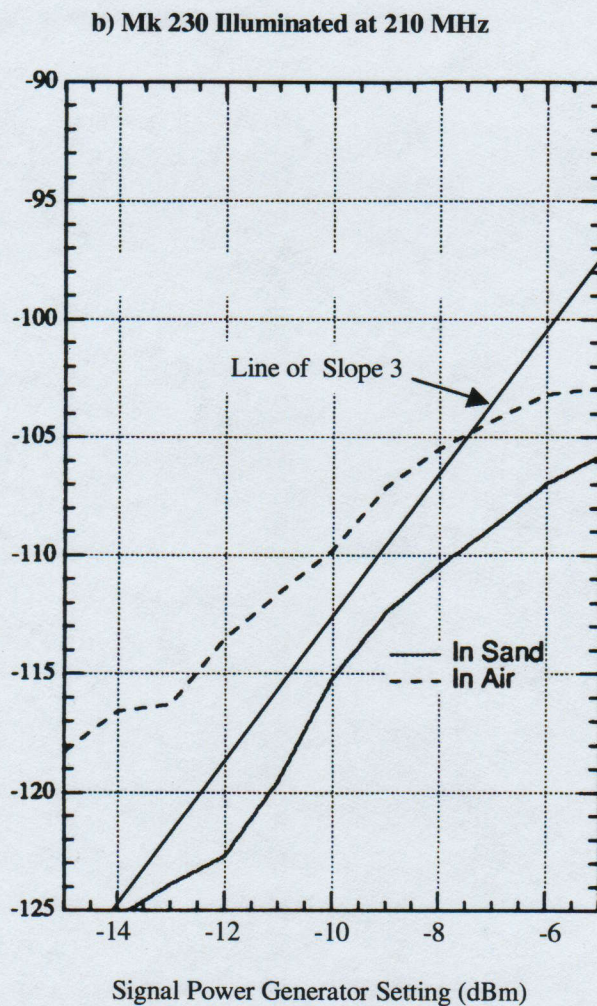
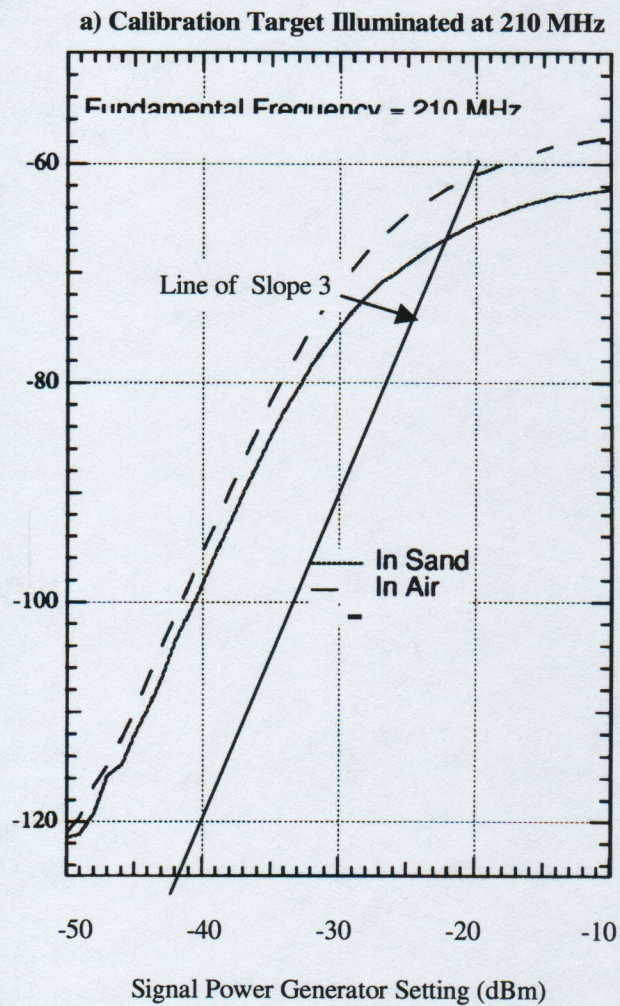


Figure 16 Third harmonic response in air and in sand.

UNCLASSIFIED

Table 3
CW Test Result Summary

Designator	Description	Maximum Response	Individual Item	Aggregates
Mk230	Hydrostatic Fuze	-83 dBm	X	X
FZ2.75	2.75" Fuze	<NF		
XM229	2.75" Warhead	<NF		
Mk40	2.75" Rocket	-95 dBm	X	X
M80	Grenade	<NF		
M42	Grenade	<NF		
G811	Grenade Body	<NF		
M879	81 mm Practice Mortar	-118 dBm	X	X
M97	Blu	-120 dBm		X
Rock	Rock Eye	<NF		
91B	Volcano 91B	<NF		
Vol	Volcano Cannister	<NF		
Mk45	Flare	<NF		
60mm	60 mm Mortar with Fins	-64 dBm		X
105	105 mm	-106 dBm		X
B250	250# Bomb Case	<NF		
Mk106	Practice Bomb	-70 dBm	X	X
Mk76	25# Practice Bomb	<NF		
M103	20 mm M103 Practice with Cartridge	<NF		
40	40 mm Projectile	-106 dBm		X
40B	40 mm Projectile (belted)			X
	Assorted Small Arms (brass)			X
	Ammo Box		X	-

Mk 106 practice bombs were individually detectable, producing signals near -70 dBm. The other UXO that were detectable individually were the Mk 230 fuzes (-83 dBm), the Mk 40 rocket motors (-95 dBm), one of the three M879 81 mm projectiles (-120 dBm), and the hinged ammunition box. All other individual pieces of UXO had responses below or near the noise floor of -125 to -130 dBm, and were judged nondetectable ("<NF" in the table).

Aggregates of UXO were more likely to produce a measurable response. The UXO that were detected when stacked included the M97 Blu (-120 dBm), the 105 mm projectiles (-106 dBm), and the 40 mm shells (-106 dBm).

Conclusions from CW Experiments. The conclusions we drew from the results are summarized as bulleted items and then discussed below.

- CW signals can produce third harmonics in some UXO
- Harmonically active UXO typically have complex structures

UNCLASSIFIED

- Aggregates of UXO are more likely to produce measurable harmonics

Third harmonics are produced by metal-to-metal joints having a dielectric (oxide, air, etc.) gap of a critical distance. Individual shells, bomb casings, and the like, do not possess these joints and are therefore poor producers of harmonics. Practice bombs, rocket motors, complex fuzes, ammo boxes, and so on, that possess hinges, springs, fins, and the like, will usually produce third harmonics. Likewise, aggregates of shells and other UXO will form casual metal-oxide-metal joints that are typically harmonically active. Usually, UXO with painted surfaces are not as harmonically active, presumably because the paint surface is too thick, although many buried UXO have rusted or deteriorated painted surfaces, which can form harmonic junctions with other such pieces.

- Third harmonic UXO response increased nonlinearly (3^{rd} power) with power levels

As discussed in Appendix A, power produced at the third harmonic typically goes as the cube of the incident power at the fundamental frequency (up to a saturation limit). Increasing the incident field improves the harmonic conversion efficiencies of the UXO up to some limit. Field levels of about 5 to 50 V/m, as produced in the chamber, seem to be about optimal.

- Harmonic conversion efficiencies varied with frequency
- Harmonic conversion efficiencies varied with polarization

The amount of harmonic energy produced by an object is critically dependent on the efficiency with which the energy at the fundamental frequency can couple into the object. This coupling is closely related to the standard radar cross section (RCS), which is dependent upon the size, shape, and orientation of the object, as well as the polarization of the radiation. Similarly, the efficiency with which any third harmonics produced by the object can be reradiated depends on its geometric properties. RCS measurements of the Mk 230⁴ as a function of frequency were consistent with its harmonic efficiency curve (see Figure 15).

3.3 IMPULSE EXPERIMENTS

3.3.1 Experimental Setup

The setup for the impulse waveform experiments was similar to that of the CW waveform experiments. Figure 17 shows a block diagram for the impulse system. The transmitter, in this case, consists of a pulse generator, capable of producing 2 ns, 1 to 10 kV pulses at a repetition rate of up to 400 Hz. In the figure, note that f_1 and f_3 refer to the fundamental and third harmonic frequency bands, respectively. The output spectrum of the pulse generator has peak energy nominally in the 200 to 400 MHz band, with a $1/f$ fall-off at higher frequencies.

⁴ A table summarizing the standard RCS measurements of most of the UXO is included as Appendix B.

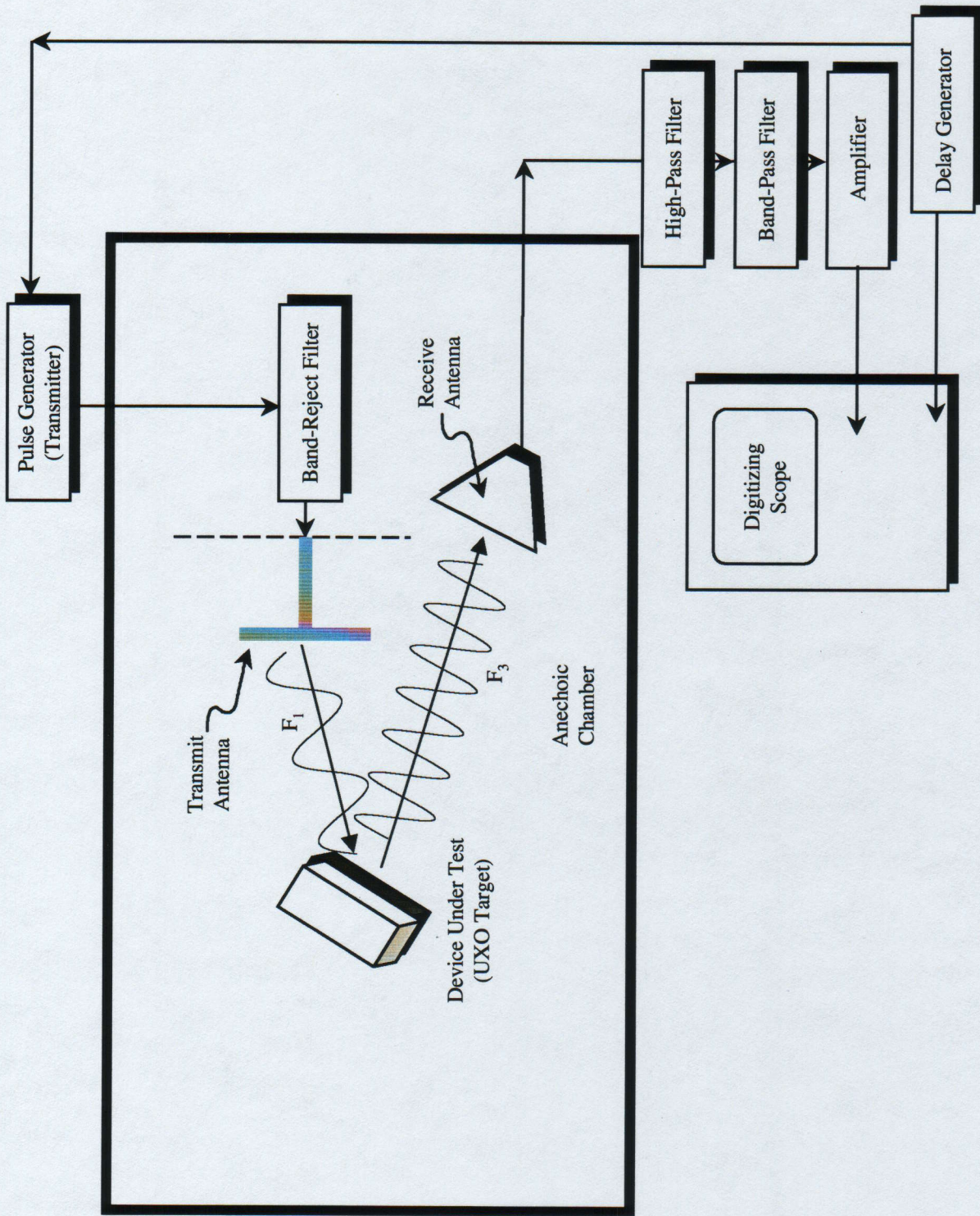


Figure 17 Impulse measurement system block diagram.

UNCLASSIFIED

To remove the energy from the impulse waveform that lies in the third harmonic band (600 to 1200 MHz), a band-reject filter, capable of handling the high voltages of the pulses, was specially designed and built by SRI. Figure 18 shows the frequency response of the filter. In the passband, the VSWR was less than 0.3 dB, while the notch in the reject band was -90 to -100 dB. Figure 19 shows the spectral content of the impulse source without (a) and with (b) filtering. In Figure 19b, the spectrum begins to decrease in intensity at about 500 MHz and is at the noise floor by about 600 MHz. In use, the filter was soldered directly to the transmit antenna to prevent the production of spurious harmonics that would be produced by connectors.

On the receive side, the signal was high-pass filtered (as before), but was followed by an adjustable band-pass filter to limit the bandwidth (kTB) noise, a low-noise preamplifier to amplify the low level broadband signal, and a fast digitizing signal analyzer (a Tektronix DSA-602) to record the very fast response. In order to increase SNR, we would incoherently average the responses over hundreds of pulses. To minimize integration losses caused by jitter, the DSA-602 was triggered by an attenuated and filtered sample of the pulse generator signal.

Figure 20 shows the spectrum of the impulse source (a) and a typical third harmonic broadband response (b). These data were taken following a 500 MHz high-pass and a 580 to 780 MHz band-pass filter. Note the leak-through of the fundamental signal despite the front-end filtering in the receive chain.

The geometry of the test chamber setup was kept as close as possible to that used in the CW experiments.

3.3.2 Experimental Procedure

Impulse System Calibration. Calibration of the impulse system was more difficult than in the CW case because the time response of the E-field meter was orders of magnitude too slow for the nanosecond pulse lengths of the impulse generator. An indirect calibration was therefore used.

First, the E field at the test area was measured using the E-field meter and the CW source (as described above). This calibration was then transferred to the impulse source via fundamental spectral measurements using a 24" sphere in the target area. The process consisted of using the DSA-602 to measure the response detected from first the CW, and then the impulse source at given spectral lines. Since the resulting E field was known for the CW signal, an equivalence allowed us to derive the E field resulting from the fast impulse. Figure 21 shows the three components of the E field for a given setting on the pulse generator.

The transfer function from the test area to the measured levels at the DSA-602 were similarly derived, so that third harmonic conversion efficiencies were able to be derived from the impulse waveform data.

UNCLASSIFIED

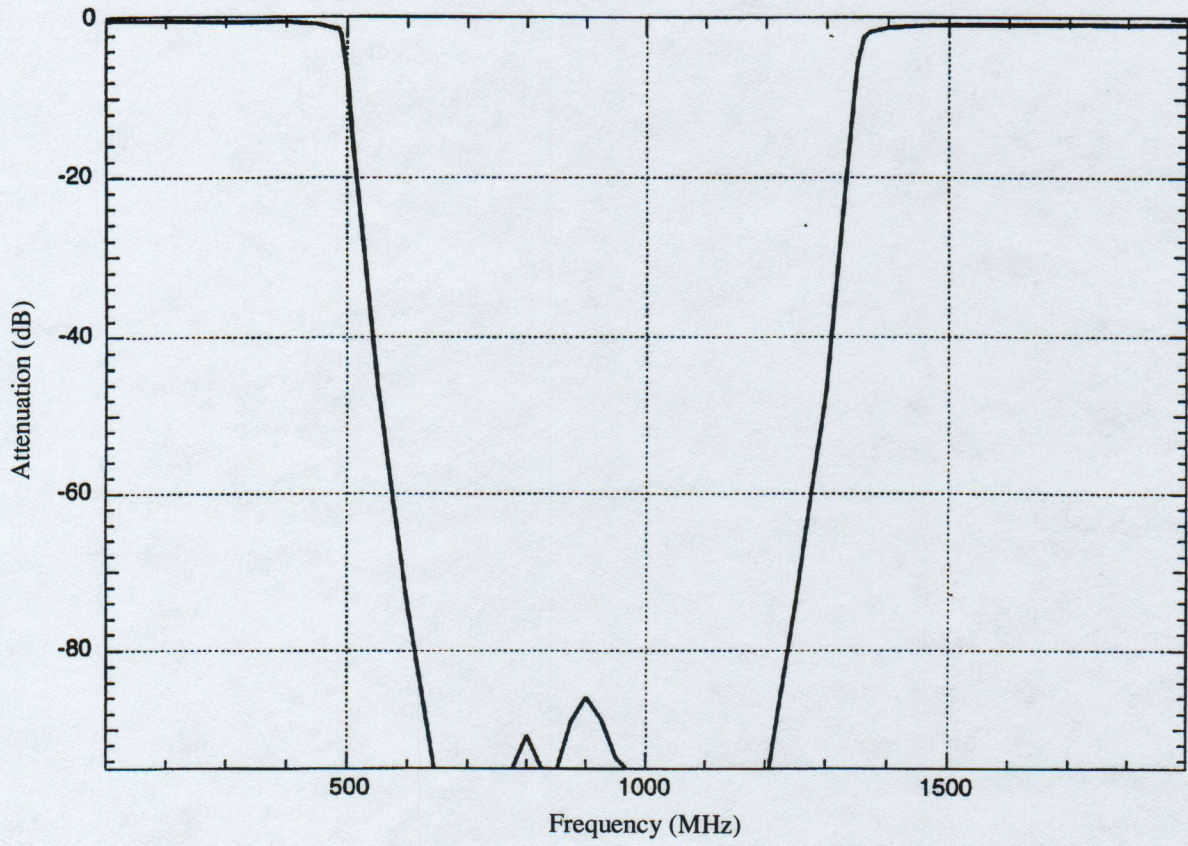


Figure 18 Band-reject filter characteristic.

UNCLASSIFIED

UNCLASSIFIED

a) Impulse Spectrum Without Filtering



b) Impulse Spectrum With Filtering

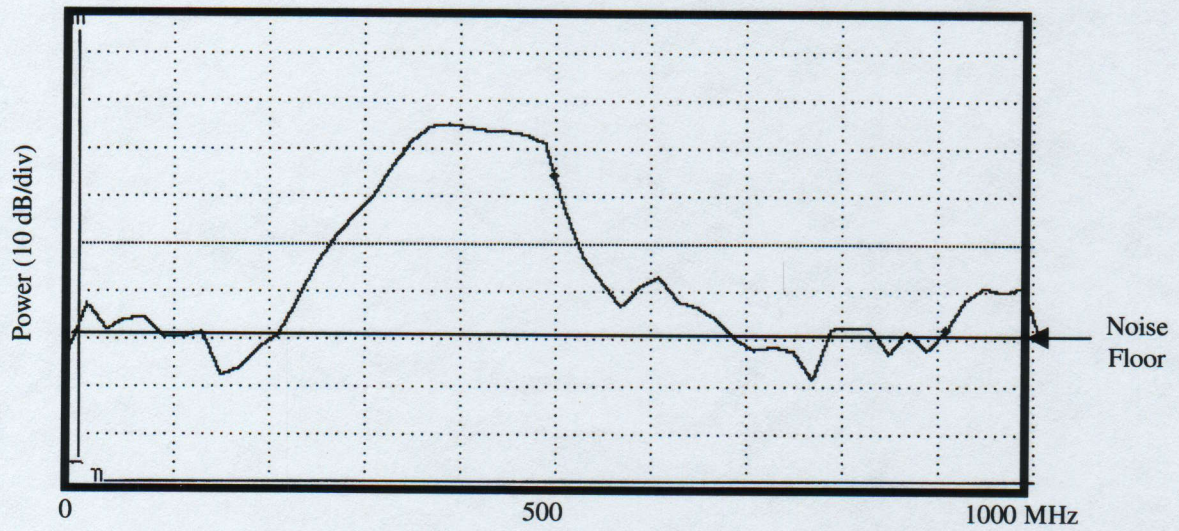
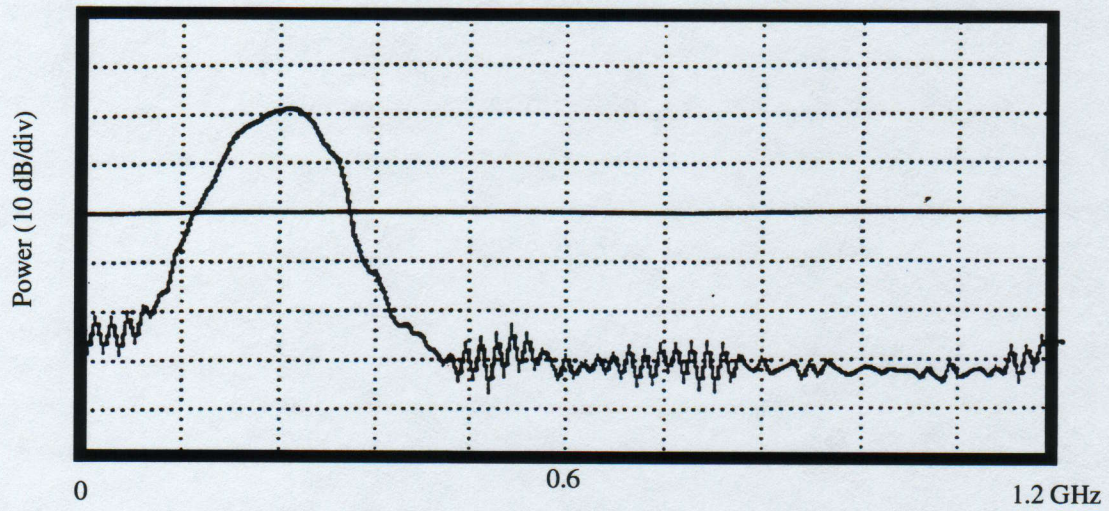


Figure 19 Impulse spectrum filtering.

UNCLASSIFIED

UNCLASSIFIED

a) Incident Impulse Spectrum



b) Third Harmonic Response Spectrum (band-pass filtered)

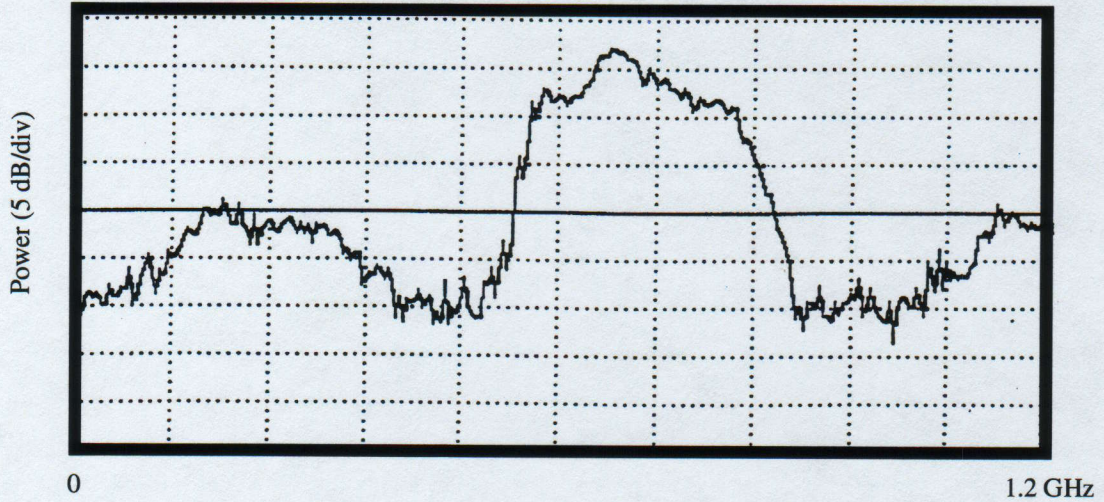


Figure 20 Wideband excitation and third harmonic response.

UNCLASSIFIED

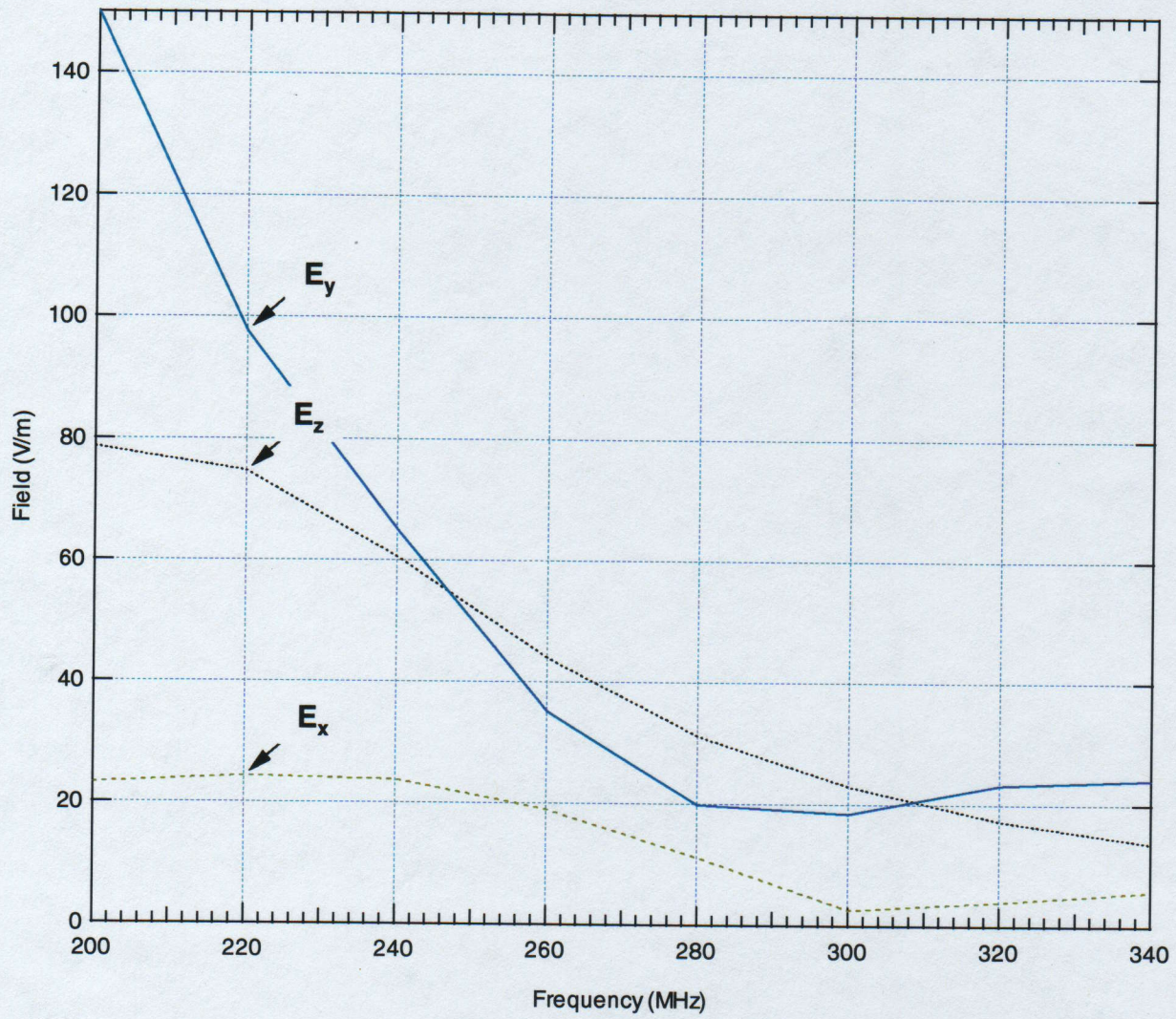


Figure 21 E field components with attenuated impulse excitation.

UNCLASSIFIED

UXO Impulse Test Procedures. The UXO third harmonic data collection procedures were similar to those described for the CW case above. In the impulse experiments, the frequency scanning was done manually on a 50 MHz wide adjustable band-pass receive filter. The power was also varied manually, by inserting HV attenuators in the transmit path. The data were digitally recorded into the DSA-602 memory and later downloaded to floppy disks.

The impulse system was inherently less stable and more prone to changes in background levels of third harmonic energy. This results mainly from the problems associated with using the much higher voltages (factor of 100) in the impulse than the CW signal. The MW peak power impulses were coupling into the receive chain and measuring equipment by various RF leakage paths. This problem was eventually solved by isolating the pulse generator in an electromagnetically shielded box with isolated and filtered AC lines, and by using only solid shield coaxial cabling, as the leakage through even double-braided cables was excessive.

At the high power levels of the impulse signal, almost any metal-metal contact or anomaly has the potential of generating nonnegligible levels of harmonics. This is the strength of the impulse approach—but also its weakness. This became even more evident with the system mounted on the radar van, when large, but intermittent, spurious harmonic signals plagued the data collection. Therefore, we retested any UXO that showed a positive response to impulse waveforms in order to confirm repeatability. The long-term data repeatability were evaluated using repeated measurements over the period of a month on both a steel wool target and one Mk 230. Based on eight separate steel wool measurements, the data were repeatable to within ± 3 dB. Ten separate Mk 230 measurements were repeatable to within ± 5 dB. The increased variability of the Mk 230 data is thought to result from the fact that it has far fewer metal-to-metal contact points than the steel wool, so that the statistical nature of the number of nonlinear junctions is more evident. Short-term repeatability was usually much better.

3.3.3 Results

Results for the impulse tests are summarized in Table 4 below. Of the 23 UXO supplied for testing, seven were shown to produce measurable third harmonic responses to impulse excitation, in the test frequency range.

With adequate short-term stability and sufficient dynamic range, we were able to measure the sensitivity of conversion efficiency with respect to incident field strength. Conversion efficiency is defined as the ratio of effective radiated, third harmonic E field to incident E field in the target area. The columns in Table 4 show similar information as was illustrated in Table 3, except that conversion efficiency is quoted here instead of maximum response.

UNCLASSIFIED

Table 4

Impulse Test Results Summary

Designator	Description	Conversion Efficiency	Individual Item	Aggregates
Mk230	Hydrostatic Fuze	-70	X	X
FZ2.75	2.75" Fuze			
XM229	2.75" Warhead	<NF		
Mk40	2.75" Rocket	<NF		
M80	Grenade	<NF		
M42	Grenade	<NF		
G811	Grenade Body	<NF		
M879	81 mm Practice Mortar	-88	X	X
M97	Blu	<NF		
Rock	Rock Eye	<NF		
91B	Volcano 91B	<NF		
Vol	Volcano Cannister	<NF		
Mk45	Flare	<NF		
60mm	60 mm Mortar with Fins	<NF		
105	105 mm	<NF		
B250	250# Bomb Case	-84	X	X
Mk106	Practice Bomb	-85	X	X
Mk76	25# Practice Bomb	<NF		
M103	20 mm M103 Practice with Cartridge	-84		X
40	40 mm Projectile	<NF		
40 B	40 mm Projectile (belted)	-63		X
	Assorted Small Arms (brass)	-68		X
	Ammo Box	-	X	-

3.3.4 Conclusions

The conclusions reached for CW waveforms (see Section 3.2.5 above) applied to the impulse waveforms, as well. However, the impulse laboratory measurements were more difficult to perform than the corresponding CW ones. The HV pulses required more custom components and special shielding arrangements, the short duration (wideband) of the pulses demanded faster (and less precise) measurement systems, and the wide receive bandwidths raised the noise floor of the receiver. We had hoped that the higher E fields generated by these pulses would produce higher harmonic responses and thus make their use worth the extra problems.

This turned out not to be the case. With the single exception of the M103, the CW system detected all of the UXO items that the impulse system detected, but it also detected some items that the impulse system missed. The loss of SNR because of the extra filtering, mismatches,

UNCLASSIFIED

thermal noise, and jitter in the system seemed to balance out any gains inherent in using the higher E fields. It is possible to design and build a more elaborate (and expensive) impulse system that may show benefits over a CW approach, but in the absence of standoff measurement requirements, this approach does not appear to be cost effective.

UNCLASSIFIED

4 VAN EXPERIMENTS

4.1 RADAR VAN SYSTEM

In the second stage of this work, the test equipment was augmented and deployed on a converted van, configured as a two-channel side-looking impulse SAR to be used to collect data on buried UXO at a government site. Figure 22 shows a block diagram of the two-channel radar. The first channel consists of a modified implementation of SRI's previously deployed impulse GPR. This conventional radar channel is tuned to the same frequency band in both the transmit and receive chain. Figure 23 shows an image of buried landmines that had been taken with this conventional SAR on a previous project. The second channel receives energy in a tunable portion of the third harmonic band.

Figure 24 shows a photograph of the radar van on site. Note the three side-looking antennas: the two large ones are the transmit and fundamental receive antennas, while the smaller one is the third harmonic receive antenna. Since a single transmitter chain is common to both receive channels, images formed from the two channels are perfectly registered. Whereas all radar targets would be imaged by the conventional system (channel 1), only targets that were active producers of third harmonics would also be imaged by the second channel, giving a basis for target discrimination.

In operation, a programmable odometer was used to enable the trigger signal from the coherent synchronizer so that sequential pulses were evenly spaced along the direction of travel.

4.2 LOCAL TESTING

Local testing at SRI, Menlo Park, showed that two-channel processing could be successful. A scene consisting of several bright radar targets, only one of which was a strong producer of third harmonic energy, was imaged by the two-channel SAR. Figure 25a shows the ortho-rectified image produced by the conventional (fundamental) receiver data of a test plot at the contractor. Note the images formed by the wooden power pole as well as by the bolted retroreflectors and the third harmonic target. Figure 25b shows the image formed by the third harmonic channel. As anticipated, only the single harmonically active target is present in this image. Figure 25c shows the superimposed fundamental and third-harmonic image.

Because of the limited dynamic range of the digitizer, and because of the high levels of RFI over much of the EM spectrum of interest in the Menlo Park and surrounding area, only very strong third harmonic producers were imaged—the calibration diode target in this case. The third harmonic response from our UXO samples were too weak to be seen over the ambient interference at this site.

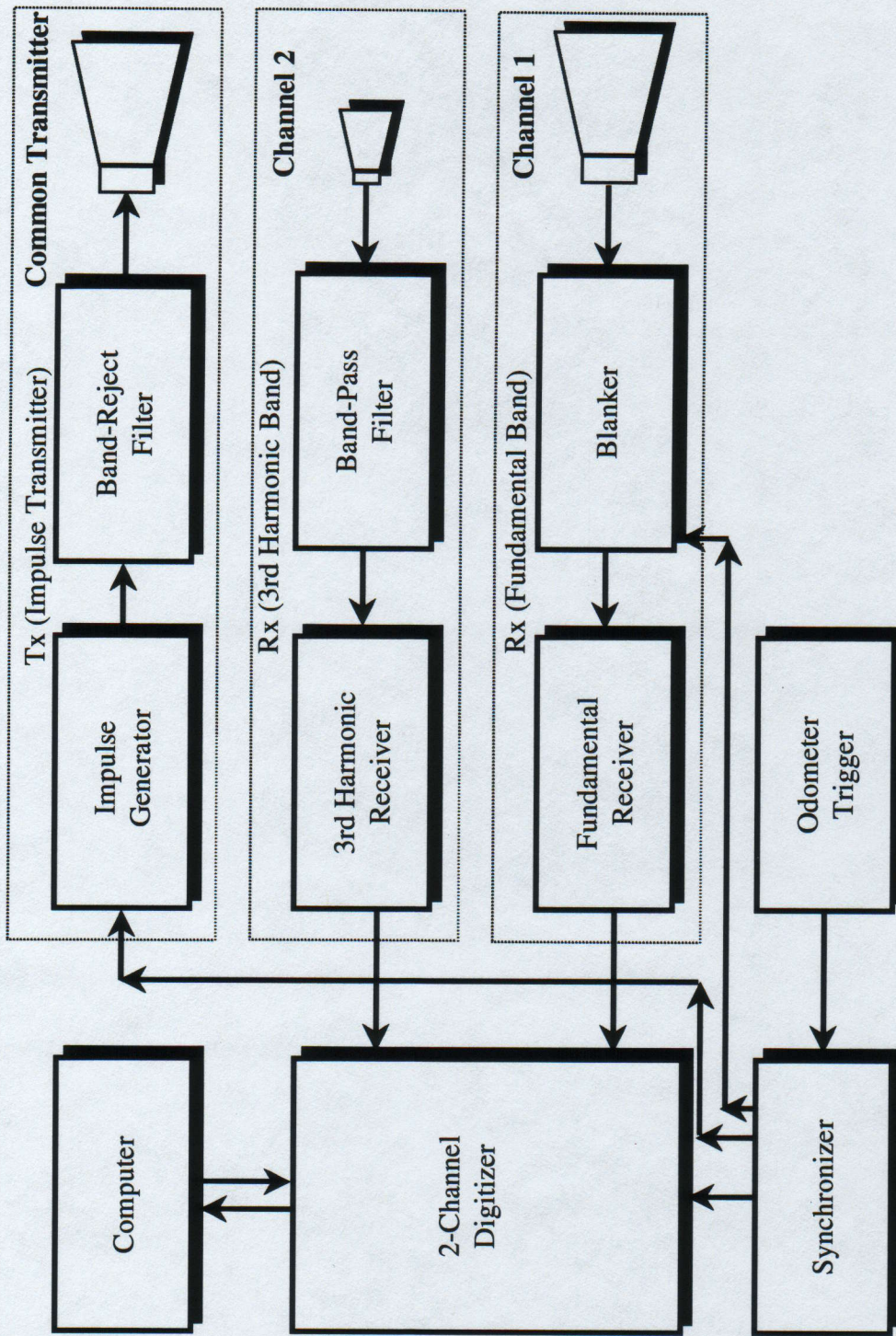


Figure 22 Two-channel van radar block diagram.

UNCLASSIFIED

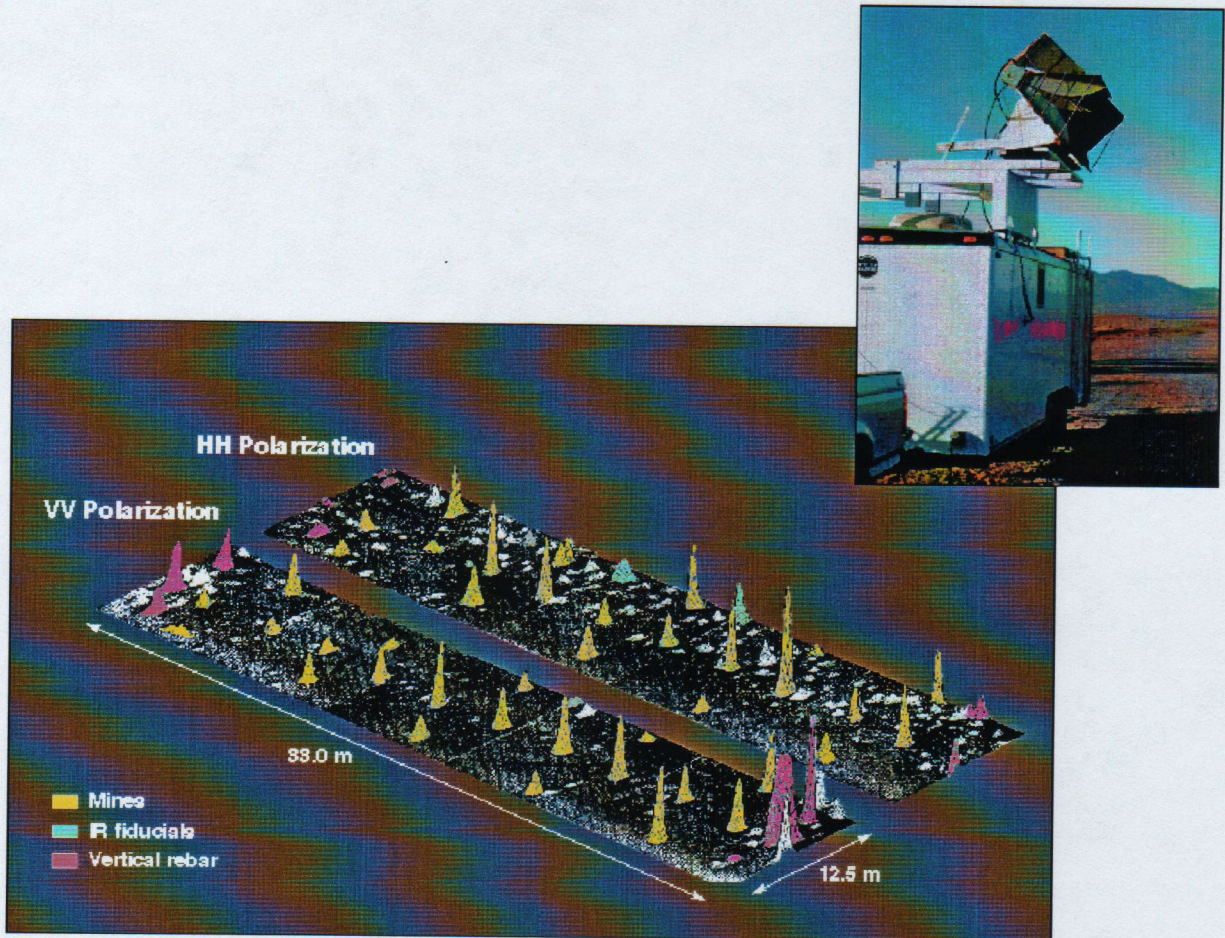


Figure 23 Image of buried mines at Nevada Test Site.

UNCLASSIFIED

UNCLASSIFIED

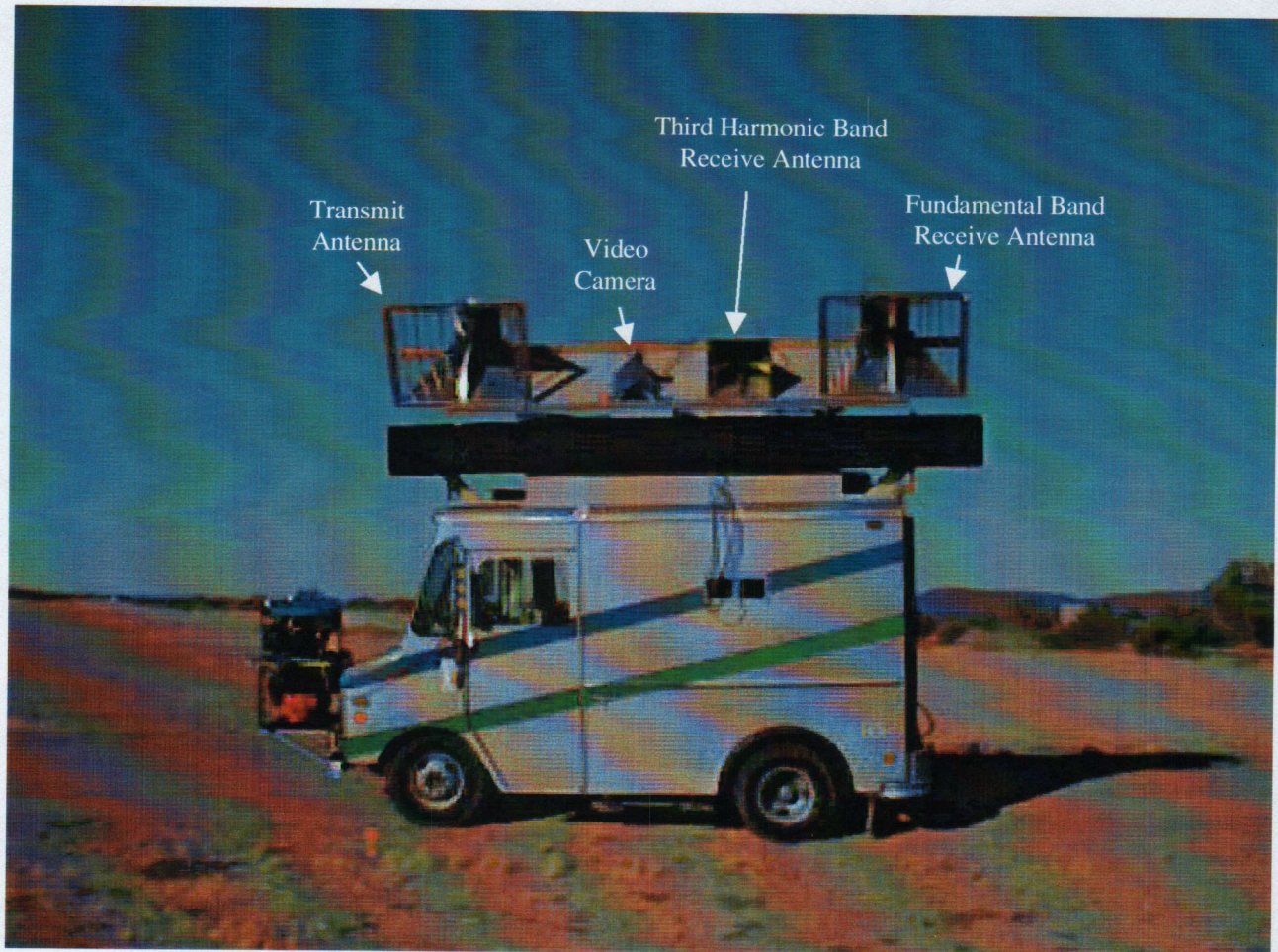
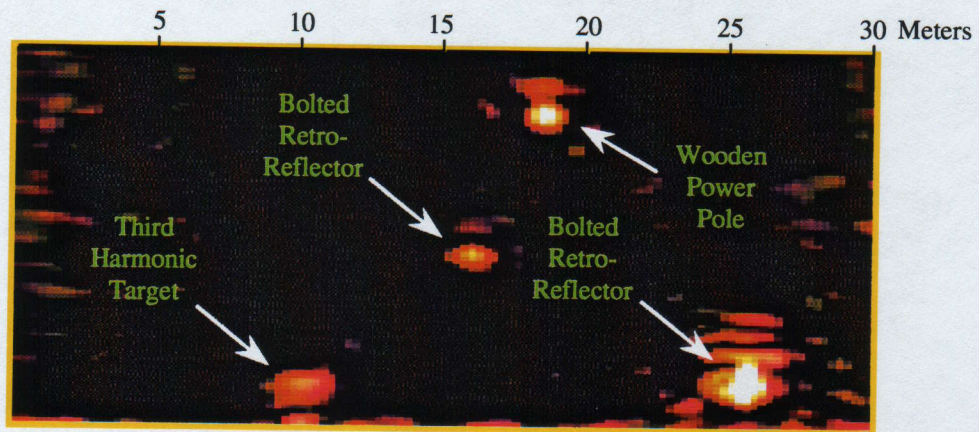


Figure 24 Side-looking two-channel radar at YPG.

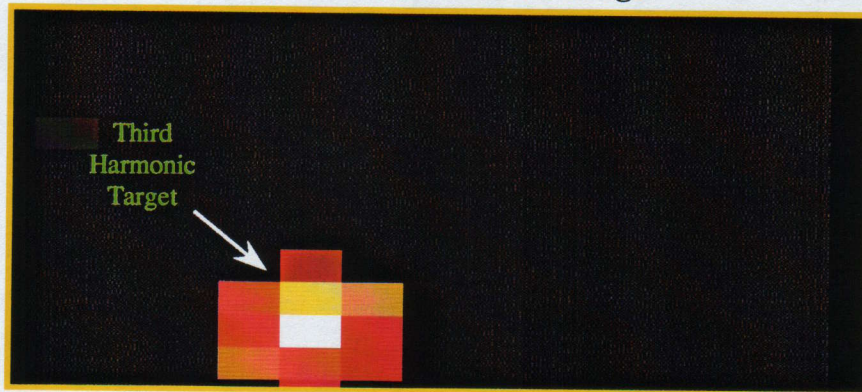
UNCLASSIFIED

UNCLASSIFIED

a) Fundamental Channel Image



b) Harmonic Channel Image



c) Overlaid Images

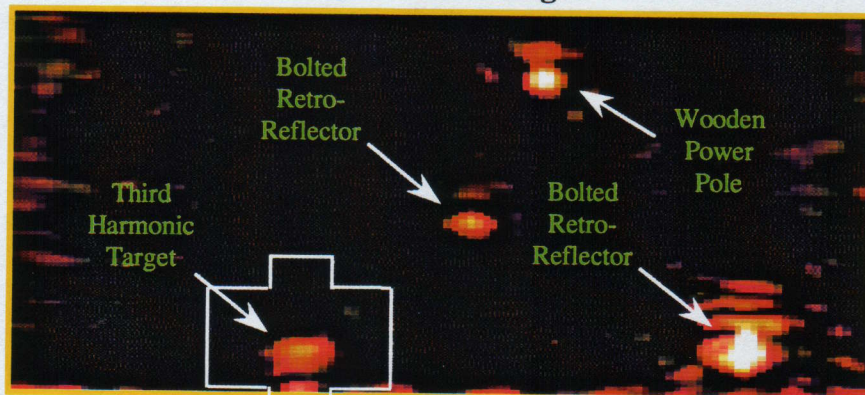


Figure 25 Two-channel impulse radar images.

UNCLASSIFIED

UNCLASSIFIED

As can be seen in Figure 25, the resolution of the harmonic radar is poorer than that of the conventional radar. Theoretically, the bandwidth of the harmonic response for the 200 MHz wide impulse system is quite large (600 MHz!) and the resolution should be at least as good as that of the fundamental channel. To achieve this resolution, we would need to have a receiver that is wide open to this very large bandwidth. It is unlikely that we would find such large bandwidths in this frequency range that are not populated by very strong interferers (radio, TV, cell phones, and other sources of RFI). Without heroic measures, it is not feasible to have enough dynamic range in the receive chain to accommodate the large bandwidth and high levels of RFI. We therefore used a tunable 50 MHz bandpass filter at the front end of the receive chain to select that portion of the band that has the lowest levels of RFI at a given site. This restriction of the bandwidth results in poorer resolution in the harmonic channel. When used in conjunction with a conventional (perfectly registered) SAR, this does not severely impact the usefulness of the system, as the harmonic radar image can be used to call attention to a region-of-interest in the high-resolution SAR image, as seen in Figure 25.

4.3 GOVERNMENT SITE TESTS AND RESULTS

The radar van was loaded on a flatbed truck and shipped to a government site at the Yuma Proving Ground in Arizona. Since the ambient RFI levels were known to be quite low at Yuma, we planned to operate the impulse system as a two-channel SAR. Having experienced problems with this system at SRI because of high RFI and intermittent spurious harmonic signals generated by the van platform itself, we also took the CW (nonimaging) probing radar system as a backup.

The YPG area in which we worked (adjacent to the Phillip's drop zone) already had some individual UXO pieces and many landmines buried and ground-truthed for other programs. A sketch of the site is shown in Figure 26. The UXO field area contained many buried landmines and a limited number of other UXO that had been emplaced for other contractors. We used the adjacent jeep trail to collect SAR data of this target area. Access to much of the site was limited as the van would tend to break through the thin desert surface and get stuck in loose sand.

A YPG crew also buried some UXO pieces and aggregates specifically for this program. These items are sketched in Figure 26; some are shown in Figure 27 placed in the surveyed holes ready for backfilling. Table 5 shows the items buried specifically for these tests. Other targets of opportunity were discovered on site, such as the crates of practice bombs and other UXO shown in Figure 28.

UNCLASSIFIED

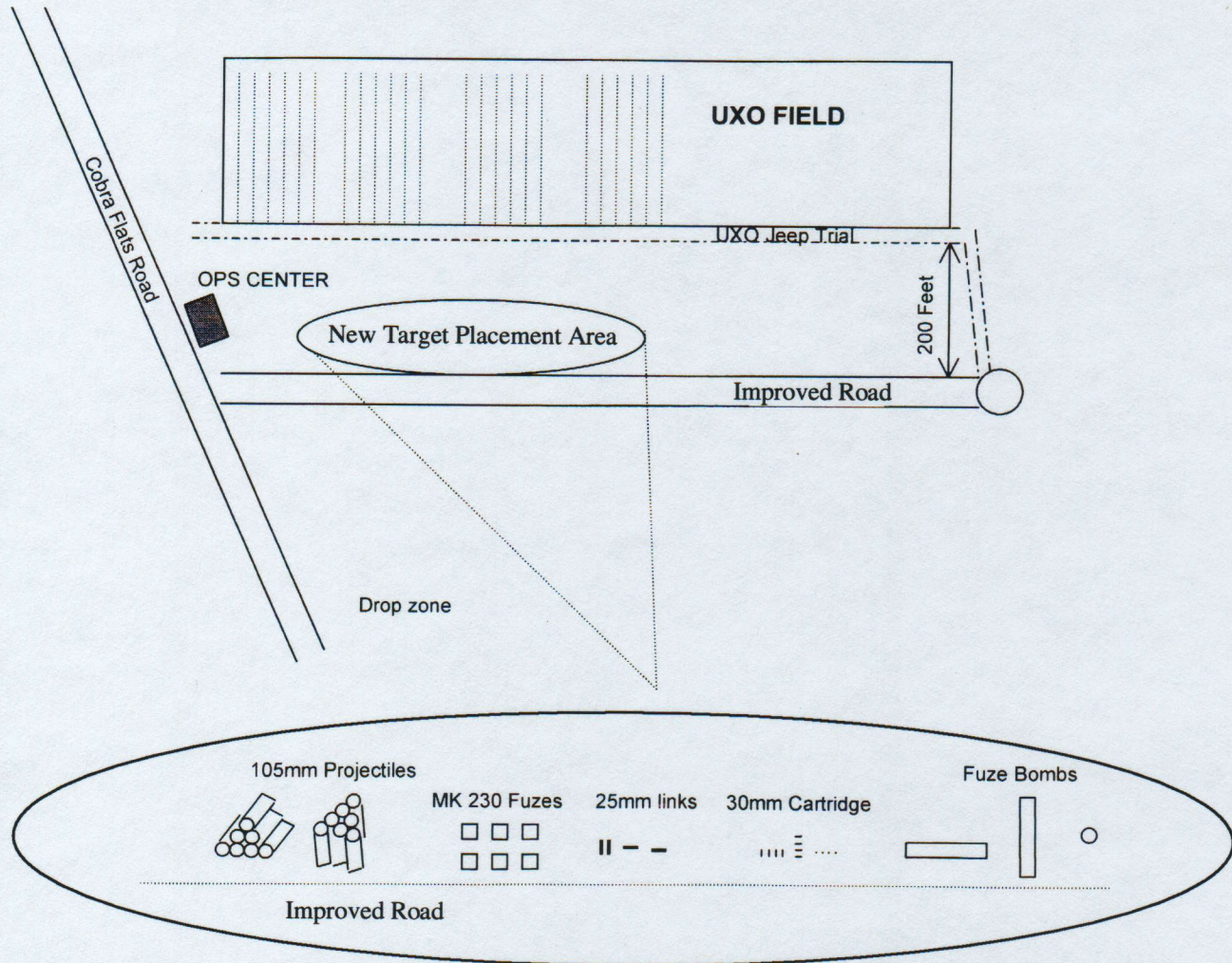


Figure 26 Site layout at YPG.

UNCLASSIFIED

UNCLASSIFIED

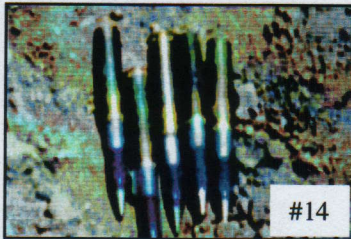
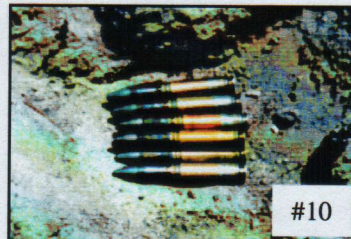
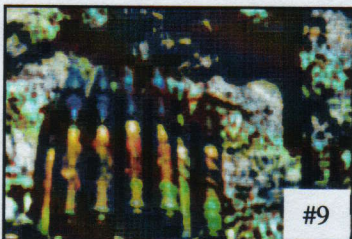
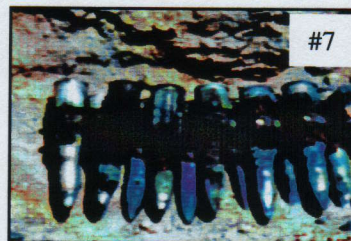


Figure 27 UXO in burial holes at YPG, ready for backfilling.

UNCLASSIFIED



Figure 28 Targets of opportunity at YPG.

UNCLASSIFIED

UNCLASSIFIED

Table 5
New UXO Buried at YPG

Designator	Description	Quantity
105 mm	105 mm Projectiles	20
Mk230	Mk 230 Hydrostatic Fuzes	16
M905	M905 Fuze Bombs with Tail	9
M848	M848 30 mm Shells	20
M103	M103 20 mm Shells	16
25 mm	25 mm Links	6

Much of the collection time was spent collecting dual-channel side-looking SAR data. Occasional large signals in the raw harmonic data were found to be caused by the spurious signals discussed above, and not by buried targets. Much time was spent in trying to track down and correct the source of these intermittent signals that corrupted the data beyond recovery. At times the radar worked consistently without these spurious interferers. The above-ground UXO pieces shown in Figure 28 were visible even in the raw harmonic data, and at one time an anomalous but reproducible harmonic signal led us to the discovery of a trip wire attached to an inert Valmara mine that we did not know was in the area. This discovery clearly verifies that harmonic radar can, in fact, be a useful tool.

In general, however, the impulse system, as configured for this test, was not robust enough to give usable data. A jitter problem in the critical firing of the impulse source made it impossible to use integration gain effectively to pull small target signals from the noise, even when the intermittent spurious signals were less of a problem. Most of the SAR data files were severely corrupted by the large, intermittent spurious third harmonic signals produced by the van, with its many vibrating metal-metal joints.

In the final collections, the impulse system was abandoned in favor of the nonimaging, CW detection system. In the step-frequency mode, data were taken with the van stationary, and the transmit antenna placed close to (about 50 cm from) the buried UXO in the "new target placement area" (see Figure 26). The target set consisted exclusively of the objects shown in Table 5 above. Some of the UXO were stacked, while others were buried in a small group, but in such a manner that they were not touching.

The 100 watt amplifier radiated energy through the transmit horn at discrete frequency steps, while a sensitive spectrum analyzer connected to the third harmonic receive horn acted as a narrowband receiver, just as in the laboratory anechoic chamber experiments. The transmit antenna was removed from the van roof and placed close to the burial positions, while the receive system (still mounted on the van) was about 10 meters away. This prevented the harmonic production of the van from swamping the UXO returns.

UNCLASSIFIED

The results from these YPG CW tests are summarized in Table 6.

Table 6

CW Results Summary from YPG

<u>UXO</u>	<u>Orientation</u>	<u>UXO Position</u>	<u>Average (dBm)</u>	<u>Signal Above Background (dBm)</u>	<u>Detection</u>
105 mm	Vertical	hole 1	-109	0	
105 mm	Parallel	hole 2	-106	4	?
Mk230	Parallel	hole 3	-112	-2	
Mk230	Parallel	hole 4	-92	17	X
Mk230	Perpendicular	hole 5	-97	13	X
Mk230	Vertical	hole 6	-96	14	X
20 mm Links	Perpendicular	hole 7	-88	22	X
20 mm Links	Parallel	hole 8	-88	21	X
30 mm Rounds	Perpendicular	hole 9	-108	2	
30 mm Rounds	Parallel	hole 10	-109	1	
Bomb Fuze	Parallel	hole 11	-93	16	X
Bomb Fuze	Perpendicular	hole 12	-95	15	X
20 mm Rounds	Perpendicular	hole 13	-108	1	
20 mm Rounds	Parallel	hole 14	-108	1	

The columns of this table display the UXO buried in each position, the orientation of the UXO relative to the horizontal E field, the average third harmonic return, this average after subtraction of the background average (-110 dBm), and whether it was over 13 dB above the average (criterion for a hit). Figure 27 showed photographs of the most of the UXO referenced in Table 6, along with the hole position number. Of the 14 UXO burial spots tested, 7 gave substantial third harmonic returns. Response from each of 7 of the most active targets averaged about 20 dB above the background levels measured among the UXO sites, over the 220 MHz range transmitted. In all, 8 of the targets had a third harmonic response that was over 20 dB above the background level for at least one transmit frequency.

A more informative way of displaying the results is presented in Figures 29 through 37. In Figure 29, the third harmonic level of the three background measurements are displayed as a function of the fundamental transmit frequency. The background measurements were taken in the same manner as those at the UXO burial site positions, except that the transmit antenna was positioned over three different locales that were known not to contain UXO. These three sets of data were averaged at each frequency to produce an average background file vs frequency. Figures 30 through 37 display the difference between data from files collected at different spots and this average background file. In other words, these plots show the CW response above the average background as a function of frequency.

UNCLASSIFIED

Figure 30 shows the difference between each of the three background files and the averaged background file, to provide a graphical representation of the variability of the signals around the mean. The RMS values of each the three graphs were about 4, showing that the average background is known to about ± 4 dB at any given frequency.

Figure 31 shows the plots of the third harmonic response above the background for the seven files that were considered nonhits (at holes 1, 3, 9, 10, 13, and 14). These traces have almost a zero mean and RMS values from about 3 to 5, showing characteristics much like the background files. These cannot be considered detections.

Figure 32 shows the plot of the response of the 105 m projectiles buried in hole #2, which has an average value of 4 dB above the background. However, its statistics are quite different than for the typical nonhit items of Figure 31. At several frequencies, these UXO show a response of greater than 10 dB above the background, and at 270 MHz a response of 22 dB above the background.

Figure 33 shows the two traces for the buried Mk230s in holes #4 and #5, oriented parallel and perpendicular, respectively. The response from the parallel oriented Mk230 is expected to be greater than that of the perpendicularly oriented items, although the data show frequencies at which this is reversed. Significantly, the two curves have very similar shapes as a function of frequency—suggesting a spectral signature for this type of UXO. The spectral response around the peak at 260 MHz also matches the in-air spectral response of the Mk230 (see Figure 15).

Figure 34 shows the traces from the two data files collected, at different times, over hole #6 containing the vertically oriented Mk230s. The traces are similar to each other, as expected, and bear a marked resemblance to the traces of the horizontally oriented Mk230s in Figure 33.⁵

Figures 35 and 36 show the results from the data files collected over holes #7 and #8, both of which contained belted rounds of 25 mm shells. The two traces of Figure 36 vary by several dB, but are similar in shape. The traces in Figure 35 are also similar to those of Figure 36, suggesting a spectral signature.

Figure 37 show the traces of the data taken at holes #11 and #12, containing the same type of bomb fuzes oriented parallel and perpendicular to the incident E field, respectively. Again, these UXO harmonic response are very similar to each other in spectral response—indicative of a harmonic spectral signature.

The idea of a harmonic spectral signature for harmonically active UXO is exciting, but requires more field verification. Unfortunately, time did not permit a more extensive data collection with the CW system. This will be performed during the next phase of the work when we return to YPG with a more efficient system. At that time we will be able to assess whether various harmonically active UXO do possess a reliable third harmonic frequency signature.

⁵ It is well to remember that individual harmonic measurements tend to vary by ± 3 dB.

UNCLASSIFIED

4.4 CONCLUSIONS

The van system showed some successes, but left some questions not fully answered. The incident where we discussed a trip were attached to a Valmara mine that we did not know was there and shows the potential of the system.

The imaging third harmonic system was shown to work, but only with very responsive third harmonic generators (e.g., the calibration diode target and the above-ground boxes of UXO shown in Figure 28). The high noise level and intermittent saturation of the impulse system due to harmonic generations on the van, itself corrupted much of the YPG data, so that standard data reduction methods were not useful.

The CW step-frequency, nonimaging third harmonic system worked quite well, but was only deployed for the last afternoon at YPG and tested only at a limited number of locations. The data were quite consistent and easy to interpret, although more work needs to be done to determine if frequency signatures in the third harmonic band are a reliable discriminant for buried UXO.

UNCLASSIFIED

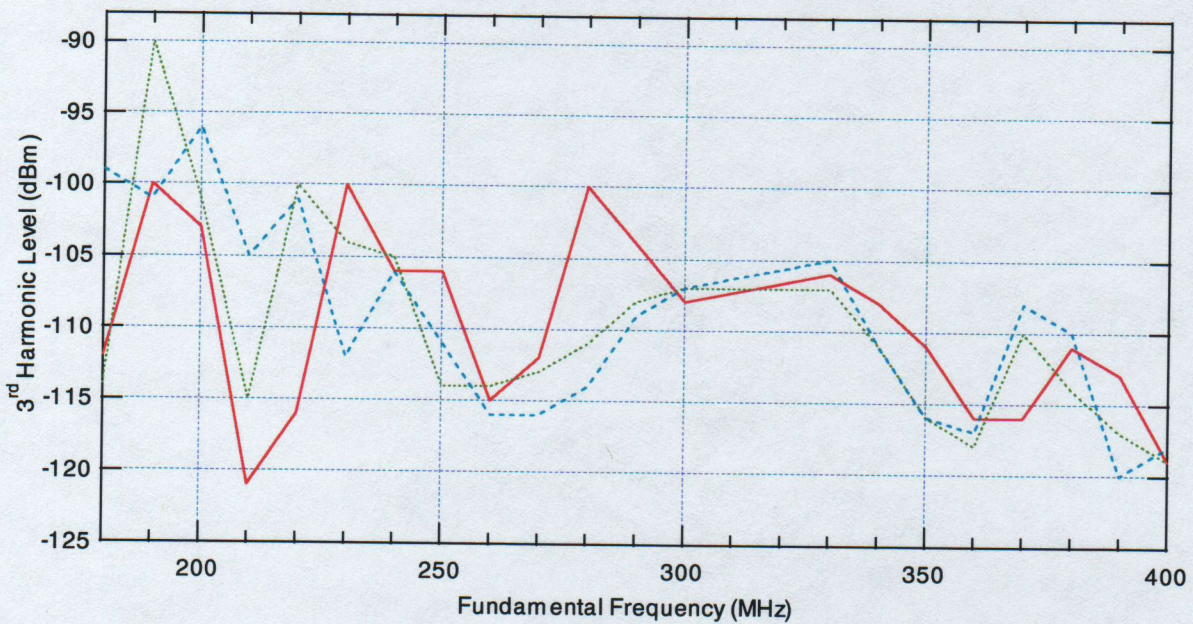


Figure 29 Third harmonic background levels at YPG.

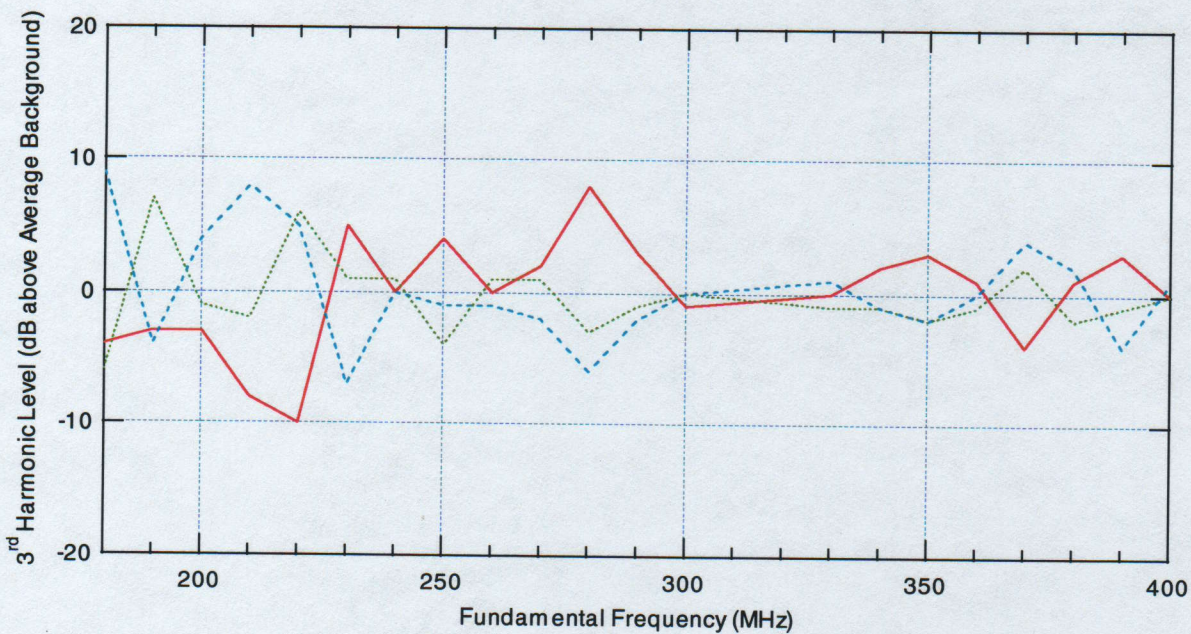


Figure 30 Third harmonic background response variance.

UNCLASSIFIED

UNCLASSIFIED

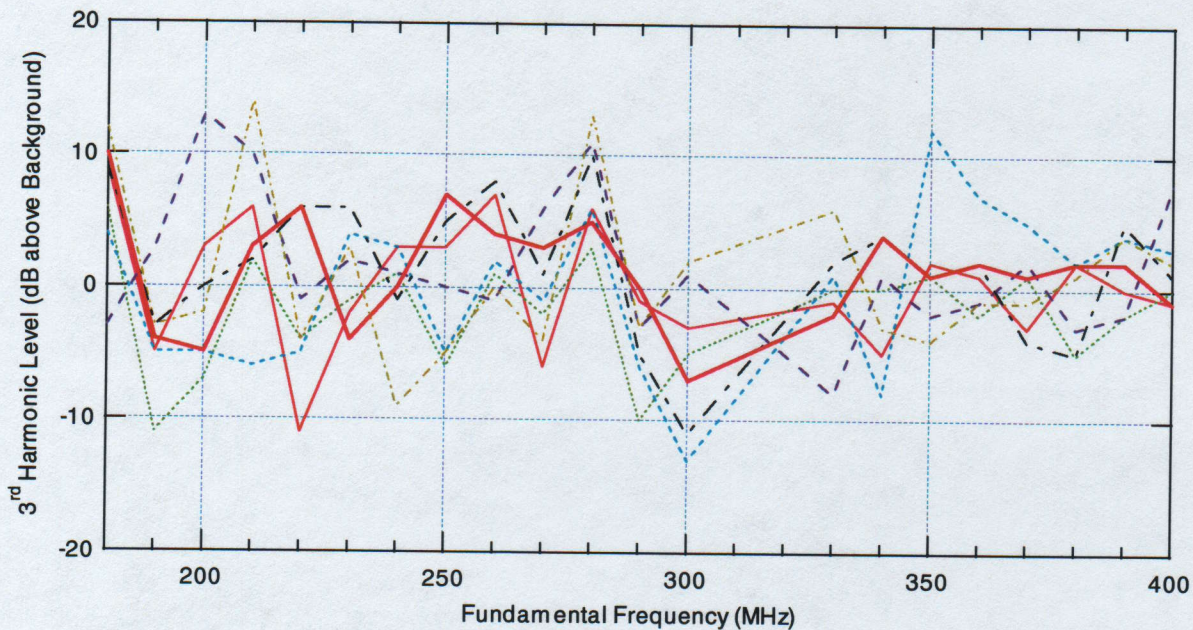


Figure 31 Third harmonic CW response of UXO not detected.

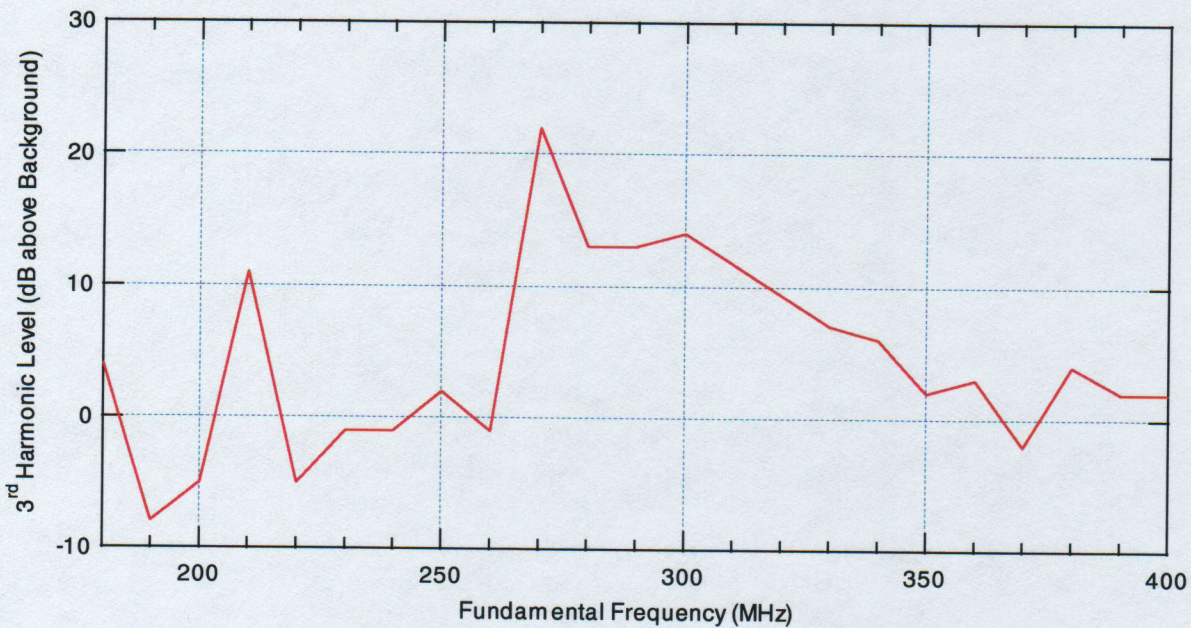


Figure 32 Third harmonic CW response of 105M projectiles.

UNCLASSIFIED

UNCLASSIFIED

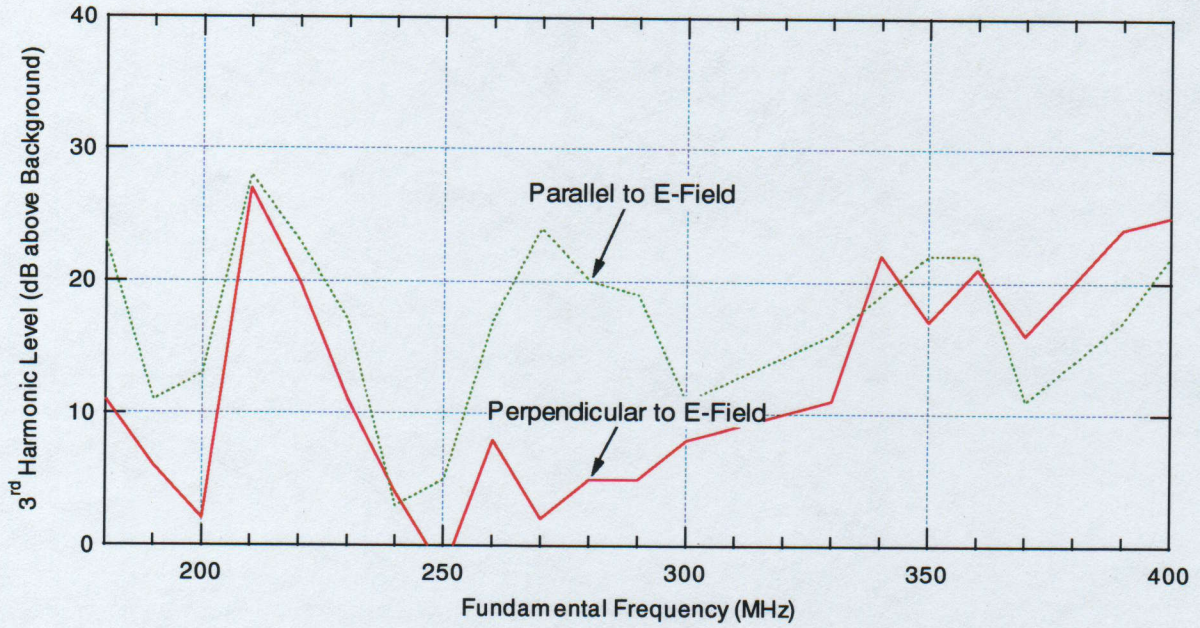


Figure 33 Third harmonic CW response of horizontal Mk 230s.

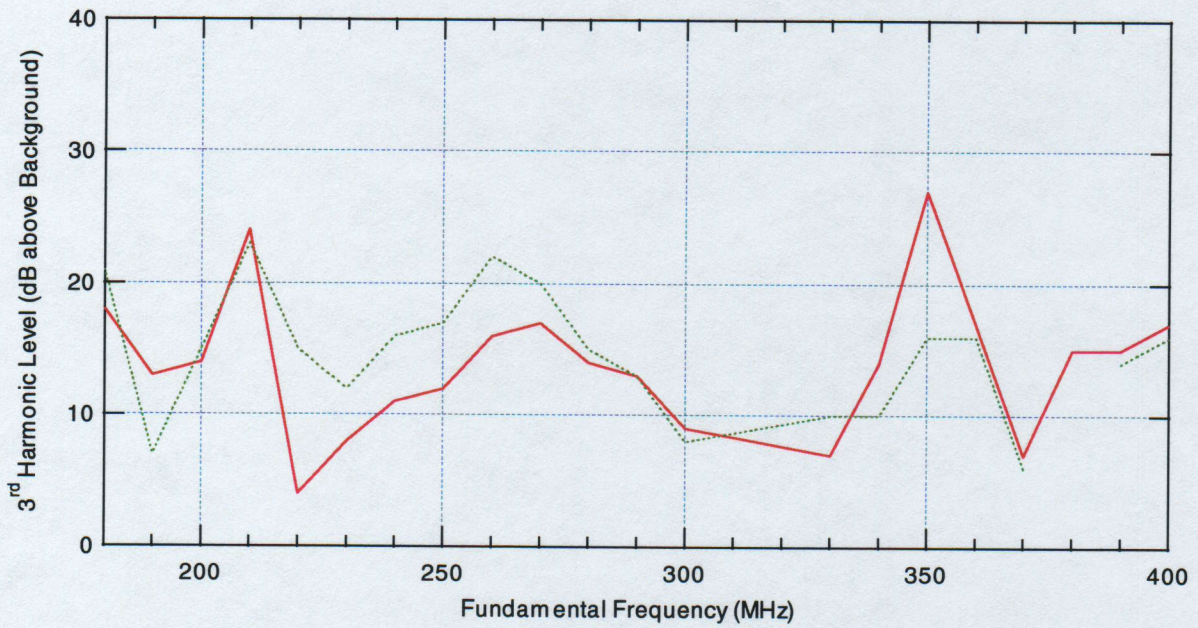


Figure 34 Third harmonic CW response of vertical Mk230s.

UNCLASSIFIED

UNCLASSIFIED

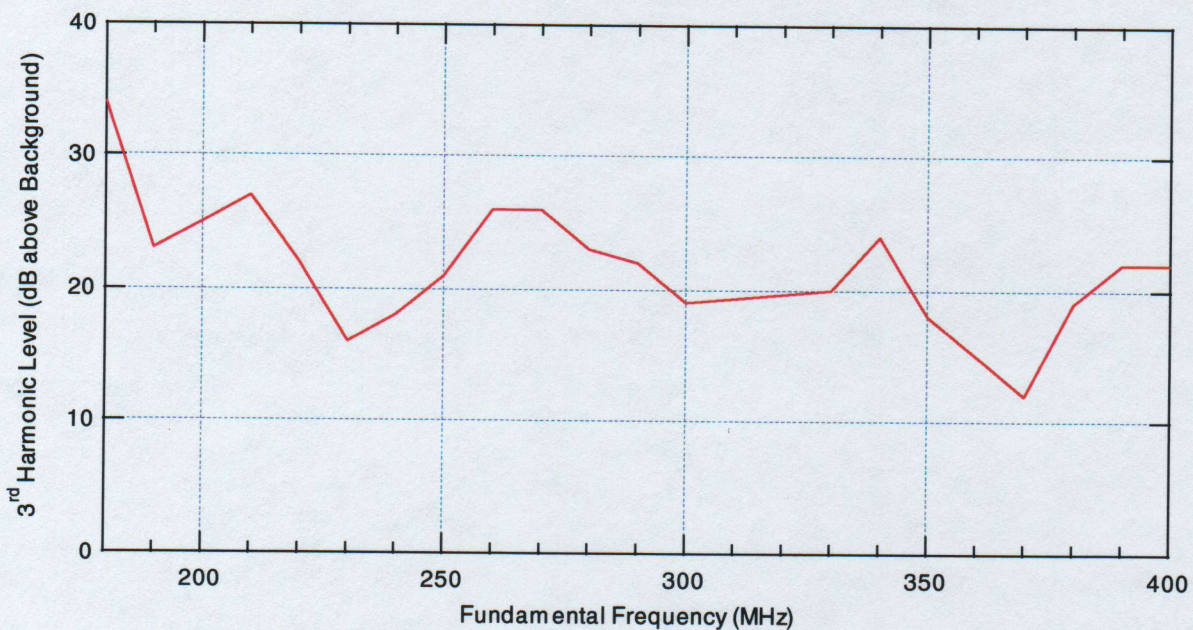


Figure 35 Third harmonic CW response of belted shells (perpendicular to E field).

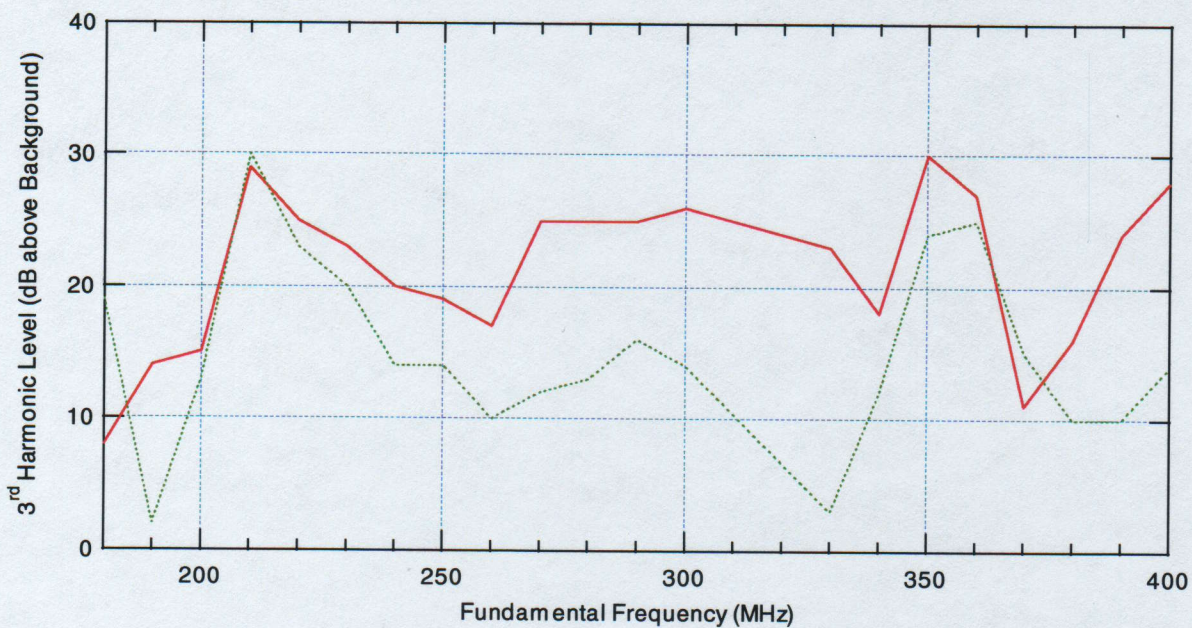


Figure 36 Third harmonic CW response of belted shells (parallel to E field).

UNCLASSIFIED

UNCLASSIFIED

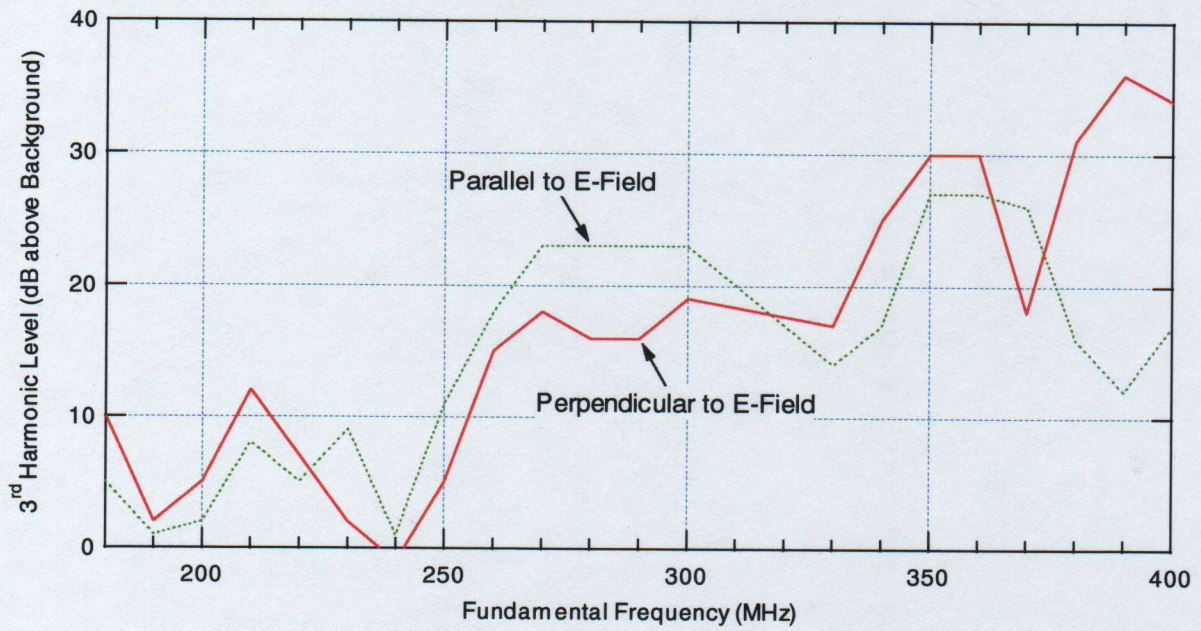


Figure 37 Third harmonic CW response of bomb fuzes.

UNCLASSIFIED

UNCLASSIFIED

5 CONCLUSIONS AND LESSONS LEARNED

- Some UXO items are harmonically active and can be found with an appropriate third harmonic radar system at close range.
- Aggregates of UXO, or UXO fragments, have a better chance of producing harmonics.
- The 100 to 400 MHz fundamental frequency range is probably best for buried UXO—both because of ground-penetrating properties and harmonic production efficiency.
- Some of the data suggest that the harmonically active UXO possess a frequency signature. This effect could help identify the buried ordnance. More work needs to be done in this area before this effect can be properly verified and evaluated.
- A stepped-frequency CW radar is more appropriate than an impulse system for UXO detection and discrimination in the US. Appendix C has a more thorough discussion of this conclusion.
- Many individual UXO items produce only subnoise level third harmonics and will escape detection by a purely harmonic type of radar.
- Third harmonic radar would, by itself, miss many UXO targets and should not be used as a primary sensor.
- Third harmonic radar can provide an added dimension of information to a suite of sensors, particularly in the identification of hits.
- A fairly simple and efficient harmonic radar system could be deployed, as part of a sensor suite, on a programmable platform.

UNCLASSIFIED

APPENDIX A—ORIGIN OF THIRD HARMONIC RESPONSES

When electromagnetic energy of a given frequency ω impinges on an object, the time-varying EMF at the object causes time-varying currents to flow which, in turn, results in radiated energy. It is this radiation that is detected by a radar receiver as an "echo." The RCS and frequency response of the object are a function of geometry and electrical properties of the object. The details and extent of intermodulation and harmonic frequency reradiation can also be traced to the EM properties of the target.

For a strictly linear (electromagnetically speaking) target, the currents induced are directly proportional to the induced voltage; that is, Ohm's law, $I = GV$, holds.

If the EMF is produced by a pure CW tone, then V can be expressed simply as

$$V = k \sin \omega t \quad . \quad (A-1)$$

We will be interested in the response to broadband excitation as well as the simpler CW case, so we will also follow what happens when two tones are used as excitation. This case will later be generalized to a continuous spectrum.

If the EMF is produced by a two-tone radar, then V can be expressed as⁶

$$V = k_1 \sin \omega_1 t + k_2 \sin \omega_2 t \quad , \quad (A-2)$$

with the resulting current

$$I = Gk_1 \sin \omega_1 t + Gk_2 \sin \omega_2 t \quad , \quad (A-3)$$

so that reradiation occurs only at the two incident frequencies ω_1 and ω_2 .

Ohm's law is, however, only a special case of expressing the induced current as an infinite Taylor's expansion in voltage:

$$I = G_0 + G_1 V^1 + G_2 V^2 + G_3 V^3 + \dots \quad . \quad (A-4)$$

Substituting Eqn. (A-2) in Eqn. (A-4) results in

$$I = \sum_{n=0}^{\infty} G_n (k_1 \sin \omega_1 t + k_2 \sin \omega_2 t)^n \quad , \quad (A-5)$$

⁶ In a complete description, an arbitrary phase angle would be included. The analysis for our purposes remains the same, and the phase angle is left out for simplicity.

UNCLASSIFIED

where n is an integer equal to the "order" of the process. For second-order and higher processes ($n > 1$), Eqn. (A-5) will contain cross product terms of the form

$$c(\sin \omega_1 t)^{n-m} (\sin \omega_2 t)^m \quad \text{with } n, m \text{ integers, and } n \geq m \quad . \quad (\text{A-6})$$

It is these terms that produce the frequency mixing, resulting in new frequencies of the form

$$\omega = n_1 \omega_1 \pm n_2 \omega_2 \quad \text{with } n_1, n_2 \text{ integers} \quad . \quad (\text{A-7})$$

It is instructive to expand Eqn. (A-5) for the cases of a pure second- and a pure third-order target (i.e., with responses $I = G_2 V^2$, and $I = G_3 V^3$, respectively). For the pure *second-order* case,

$$I = G_2 (k_1 \sin \omega_1 t + k_2 \sin \omega_2 t)^2, \text{ which expands to}^7$$

$$I = a_0 \sin^2 \omega_1 t + a_1 \sin \omega_1 t \sin \omega_2 t + a_2 \sin^2 \omega_2 t \quad . \quad (\text{A-8})$$

Using the trigonometric identities

$$\sin^2 \omega = \frac{1}{2} [1 - \cos 2\omega], \text{ and}$$

$$\sin \omega_1 \sin \omega_2 = \frac{1}{2} [\cos(\omega_1 - \omega_2) - \cos(\omega_1 + \omega_2)] \quad ,$$

we can show that a second-order process (Eqn. [A-8]⁸) will produce only frequencies of $2\omega_1, \omega_1 \pm \omega_2$, and $2\omega_2$.

For the pure *third-order* case, Eqn. (A-5) becomes

$$I = G_3 (k_1 \sin \omega_1 t + k_2 \sin \omega_2 t)^3 \quad .$$

Expanding (and again ignoring the exact value of the coefficients), we get

$$I = b_0 \sin^3 \omega_1 t + b_1 \sin^2 \omega_1 t \sin \omega_2 t + b_2 \sin \omega_1 t \sin^2 \omega_2 t + b_3 \sin^3 \omega_2 t \quad . \quad (\text{A-9})$$

⁷ We are primarily interested in the frequency terms, and so have ignored the exact value of the coefficients.

⁸ Of course, the power level of the reradiated energy goes as I^2 , but the frequency line content will be the same as for I .

UNCLASSIFIED

Using the trigonometric identities

$$\sin^3 \omega = \frac{1}{4}[3 \sin \omega - \sin 3\omega],$$

$$\sin^2 \omega = \frac{1}{2}[1 - \cos 2\omega], \text{ and}$$

$$\cos 2\omega_1 \sin \omega_2 = \frac{1}{2}[\sin(\omega_2 - 2\omega_1) + \sin(\omega_2 + 2\omega_1)],$$

we can show that for this case (a third-order process) the reradiated spectrum will contain only frequencies of ω_1 , ω_2 , $3\omega_1$, $3\omega_2$, $2\omega_1 \pm \omega_2$, and $2\omega_2 \pm \omega_1$.

For the case of three tones (ω_1 , ω_2 , ω_3). mixing a similar analysis can show that the reradiated spectrum will contain only frequencies of ω_1 , ω_2 , ω_3 ; $3\omega_1$, $3\omega_2$, $3\omega_3$; $2\omega_1 \pm \omega_2$, $2\omega_1 \pm \omega_3$, $2\omega_2 \pm \omega_1$, $2\omega_2 \pm \omega_3$, $2\omega_3 \pm \omega_1$, $2\omega_3 \pm \omega_2$; $\pm(\omega_1 \pm \omega_2 \mp \omega_3)$; which lie either in the fundamental band, or the third harmonic band.

The component of I (in Eqn. [A-4]) that contains one of the frequencies of interest (e.g., $2\omega_1 + \omega_2$) can thus be expressed as

$$I_{2\omega_1+\omega_2} = g_3 V^3 + g_5 V^5 + g_7 V^7 + \dots \quad (\text{A-10})$$

since these are the only terms that will contribute to the currents, and, therefore, the reradiated energy at $2\omega_1 + \omega_2$. The first term usually predominates, so we can write

$$I_{2\omega_1+\omega_2} \approx g_3 V^3, \quad (\text{A-11})$$

and the reradiated power at frequency $2\omega_1 + \omega_2$ will be proportional to the cube of the incident power level at the two tones ω_1 , ω_2 :

$$P_{2\omega_1+\omega_2} = k P_{in}^3. \quad (\text{A-12})$$

This treatment can be extended to all the third-order terms so that any frequency, f_3 , in the third harmonic band will be proportional to the cube of the incident power level.

A log-log (dB) plot of power at the third harmonic vs P_{in} should therefore be a line with a slope of 3 (see Figure 12). Of course, this relationship must break down at larger values of the incident power, since the Law of Conservation of Energy will not allow more power out than is fed in. In fact, what occurs is that the components producing the mixing will eventually saturate.

UNCLASSIFIED

APPENDIX B—UXO RCS MEASUREMENTS SUMMARY

UXO Type	View	Max. RCS (dBsm)	Frequency(s) (MHz)	Frequency Signature	Comments
Mk230 Hydrostatic Fuze	Rear	-10	800	Significant	Short period variations
	Side	-2	300	Moderate	Very large RCS
	Front	-10	800	Moderate	
2.75" Fuze	Rear	-27	1,050	Moderate	5 dB ripple in RCS @ max.
	Side	-15	1,050	Moderate	3-5 dB ripple in RCS @ max.
	Front	-27	1,050	Moderate	
2.75" Warhead (XM229)	Rear	-26	400;650;950	Significant	Significant ripple
	Side	2	230	Moderate	Very large RCS
	Front	-27	400;650;930	Significant	Significant ripple
2.75" Rocket Mtr Housing	Rear	0	370	Significant	Very large RCS
	Side	4;6	350;520	Significant	Very large RCS
	Front	1;-3	340;520	Significant	Very large RCS
M-80 Grenade	Rear	-35	320	Minimal	Low RCS
	Side	-23	1,100	Moderate	22 MHz, 10 dB ripple
	Front	-32	340	Minimal	Low RCS
M-42 Grenade	Rear	-28	1,100	Moderate	Low RCS, increasing with freq.
	Side	-20	1,100	Minimal	Low RCS, increasing with freq.
	Front	-28	1,100	Moderate	
Grenade Body Pract G811	Rear	-23	1,100	Minimal	Low RCS, increasing with freq.
	Side	-23	1,100	Minimal	Low RCS, increasing with freq.
	Front	-23	1,100	Minimal	Low RCS, increasing with freq.
81 mm M879 (mortar)	Rear	-22;-19	720;1,100	Minimal	Low RCS, increasing with freq.
	Side	-3	350	Moderate	Large RCS
	Front	-20	1,100	Minimal	Increasing with freq.
M-97 Blu (flare)	Rear	-22	1,000	Moderate	
	Side	-2	530	Moderate	
	Front	-22	1,000	Moderate	
Rock Eye	Rear	-30	Flat	Minimal	Low RCS, flat with ripple
	Side	-3	530	Moderate	Large RCS
	Front	-30	Flat	Minimal	Low RCS, flat with ripple
60 mm Mortar	Rear	-22	600	Moderate	
	Side	-3	340	Significant	
	Front	-22	600	Moderate	
Mk106 Practice Bomb	Rear	-15;-10;-12	400;700;1,020	Significant	
	Side	1;-5;-9	230;700;1,100	Significant	
	Front	-14;-10;-12	520;660;960	Significant	
Mk76 25# Practice Bomb	Rear	-16;-8	380;700	Significant	Large RCS
	Side	-1;-5	200;680	Moderate	
	Front	-16;-9;-9	340;660;800	Significant	
20 mm M103 with Cartridge	Rear	-37	Flat	Minimal	Low RCS, flat with ripple
	Side	-9	800	Moderate	Low RCS, flat with ripple
	Front	-37	Flat	Minimal	
40 mm Projectile	Rear	-28	1,100	Minimal	Low RCS, increasing with freq.
	Side	-17	1,100	Moderate	Increasing with freq.
	Front	-27	1,100	Minimal	Low RCS, increasing with freq.

UNCLASSIFIED

APPENDIX C—STEPPED CW VS IMPULSE WAVEFORMS

Originally, a wide swath airborne sensor was envisioned as the final product goal. Because of the severe range losses in the third harmonic radar equation, it was clear that only a high peak-power impulse waveform would have any chance of producing a large enough third harmonic response in buried UXO to be detectable at aircraft standoff distances. We therefore proceeded in Phase 1 toward researching, producing, and testing the phenomenology and components needed to build a third harmonic impulse radar.

A measurement program in a controlled RF environment (SRI's anechoic chamber) allowed us to develop the unique skills and tools necessary for working with high-voltage impulse waveforms, in the context of sensitive harmonic measuring devices. The measurements also provided us with the level of third harmonic energy that would be produced by typical UXO.

Several engineering hurdles were successfully cleared. A high-voltage band-reject filter was designed and built to suppress any harmonics produced in the transmit chain. A wideband horn antenna was also specially designed and constructed to radiate high-voltage waveforms without itself producing measurable levels of third harmonics. Finally, a custom third harmonic low-noise receiver was designed and built to amplify the low-level harmonic return energy.

Other problems remained. Almost any radar platform has the potential to produce and radiate third harmonics. While we were successful at SRI in eliminating the self-generation of third harmonics by the van, we found that the problem had returned once the equipment reached YPG. The problem was overcome once again, but the potential for new sources of third harmonics remained, as metal parts are continuously being vibrated loose. Our attempt at building a high-voltage diplexer, which would allow us to shunt the low-frequency unradiated energy (below the antenna cut-off) into a matched load, proved unsuccessful. While this engineering problem can be overcome with a little more effort, other difficulties are inherent in state-of-the-art impulse systems. The spectral content of present impulse sources follow a $1/f$ dependency and are lacking in energy at the high end of the band. Also, impulse systems, while possessing high peak power, are inherently low-average power radars. Impulse radars are intrinsically wideband, so the receivers are subject not only to ambient interference, but also to high thermal noise. In addition, the wide instantaneous bandwidths require high-speed digitizers, which are not only difficult to use, but typically have low dynamic range.

Impulse systems also have some positive features, and, while difficult, are certainly not impossible to implement, even for a third harmonic radar. In fact, for large standoff ranges, an impulse system is mandatory for a third harmonic radar. Nonetheless, our experiences in Phase 1 of this project lead us to the conclusion that a stepped CW rather than an impulse waveform should be used in Phase 2. In particular, the better test results from the CW over the impulse field trials at YPG argue for the stepped frequency approach.

UNCLASSIFIED

Stepped frequency radar designs are, for conventional radars, equivalent to impulse radars in most aspects, while avoiding many of the problems of impulse systems. In particular, a stepped frequency radar can have the same resolution and range as a conventional radar. Unlike in impulse radar implementations, the spectral balance across the entire frequency band of a stepped frequency radar can be excellent. Narrowband RF interferers can be easily stepped around or skipped. Dynamic range, which is probably the key to third harmonic detection, can be kept large with the use of narrowband 16-bit low-speed digitizers. This also holds true for a third harmonic radar at close ranges.